NANOPARTICLE-MEDIATED CONTROLLED MYOCARDIAL DRUG DELIVERY: A NEW TREATMENT FOR HYPERTROPHIC CARDIOMYOPATHY

by

MICHELLE KATHERINE MCGRATH COPELAND

DISSERTATION

Submitted in partial fulfillment of the requirements
for the degree of Doctor of Philosophy at
the University of Texas at Arlington
August 2020
Arlington, TX

Supervising Committee:

Jun Liao, Supervising Professor
Kytai Nguyen
Matthias Peltz
Yi Hong
Zui Pan

ABSTRACT

NANOPARTICLE-MEDIATED CONTROLLED MYOCARDIAL DRUG DELIVERY: A NEW TREATMENT FOR HYPERTROPHIC CARDIOMYOPATHY

Michelle Katherine McGrath Copeland, Ph.D.

The University of Texas at Arlington, 2020

Supervising Professor: Jun Liao

Hypertrophic cardiomyopathy (HCM) is a genetic disease of the sarcomere, resulting in overgrowth of the septum that separates the left and right ventricles. HCM can affect as many as 1/200 people, making it the most common genetic cardiomyopathy in the general population, as well as the most common cause of sudden cardiac death (SCD). In severe HCM cases, cardiothoracic surgeons perform septal myectomy to remove the excess tissue. However, many patients are poor surgical candidates and require

another, less invasive treatment option. In these cases, alcohol septal ablation (ASA) is performed. With ASA, cardiologists deliver pure alcohol through a catheter to the diseased area to shrink and kill the overgrown septal tissue. However, the alcohol is not targeted to the overgrown area and indiscriminately kills both diseased and healthy cells, often resulting in complete heart block and abnormal arrhythmias that may result in the need for permanent pacemakers. To combat this clinical challenge, we have designed a novel septal ablation technique using a targeted nanoparticle drug delivery system. By targeting the diseased area, we can decrease the risks involved in septal ablation. To begin, we observed the microstructural and mechanical properties of human healthy and HCM septal tissues to better understand their properties and how these may affect our delivery system. We discovered that HCM cells have a fibrotic microenvironment consisting of excessive collagen. By targeting the fibrotic collagen, we can deliver our nanoparticle system specifically to the diseased area, thereby decreasing the likelihood of killing healthy cells. This work was accomplished in three aims: (1) Ultrastructural and mechanical characterization of human healthy and hypertrophic cardiac septal tissues; (2) Nanoparticle-mediated controlled myocardial drug delivery; (3) Regulation of the spatial distribution of hypertrophic cardiomyopathy treatments using nanoparticles.

ACKNOWLEDGMENTS

I would like to express my sincere gratitude to my supervising professor, Dr. Jun Liao, who has guided me for the past 5 years and helped me lay the foundation for my future career. Dr. Liao's knowledge goes above and beyond the classroom, and I could not have gotten this far without his continual support.

I am grateful to Dr. Kytai Nguyen and the opportunity to be an NIH T32 fellow under her mentorship. She has taught me critical thinking and how to succeed as a woman in biomedical engineering.

I would like to express my deepest appreciation for my dissertation committee: Dr. Matthias Peltz, Dr. Zui Pan, Dr. Yi Hong, Dr. Kytai Nguyen, and Dr. Jun Liao. Each of my committee members contributed greatly to my research in different ways and I will always be grateful for their insights and assistance. I would like to acknowledge Dr. Matthias Peltz and Dr. Pietro Bajona from UT Southwestern who supplied materials for my research. Dr. Peltz and Dr. Bajona were instrumental in helping me understand hypertrophic cardiomyopathy, alcohol septal ablation, and the anatomy of the heart. I would also like to acknowledge Dr. Zui Pan who not only provided cells and other materials for my research, but also provided incredible advice and insights for my research and future career. I would

also like to earnestly thank Dr. Yi Hong for the many hours he contributed to help me with my research, and for the contributions he made to ensure my success.

I would also like to express my appreciation to Uday Chintapula and Deepsundar Sahoo for their constant help with my research. Uday relentlessly assisted me with my research projects, and I will always be grateful for everything he has taught me.

Many thanks to my current and previous lab members, especially Dr. Bryn Brazile and Dr. Sourav Patnaik, who encouraged me to continue my hard work, knowing that it would one day pay off. Both Dr. Brazile and Dr. Patnaik offered advice and help at all points during my Ph.D. studies, and I am eternally grateful.

I could not have completed this chapter of my life without my family's encouragement and support. Thank you from the bottom of my heart.

DEDICATION

This dissertation is dedicated to the loving memory of Betty Faye Brunt McGrath, my beloved Mimi. If she were still with us, I know she would be proud of her precious darling angel child's accomplishments.

This dissertation is also dedicated to my family:

First, I would like to put the spotlight on my favorite person in the world, my husband, Tommy Copeland. He took care of our kids without complaint at times when I was overwhelmed with work. His constant love and support are the reason I was able to finish my dissertation research.

Second, I would like to dedicate this dissertation to my beautiful girls, Autumn Katie and Rachel Ann Copeland. Coming home to their smiling faces each day was the highlight of my work week. Without knowing it, my girls encouraged me to continue so I could make a better life for them in the future.

Without help from my sister and brother-in-law, Margaret and Morgan Holland, I could not have made it this far. They sacrificed their time and resources to help me raise my children, and I will always be grateful to them. This dissertation is also dedicated to them.

Finally, I dedicate this dissertation to my mom and dad, Melinda and Hoyt McGrath, who provided me with everything I needed to succeed no matter the cost.

I love you all!

TABLE OF CONTENTS

LIST OF TABLES AND FIGURES

CHAPTER 1

INTRODUCTION AND BACKGROUND

1.1 Introduction to Hypertrophic Cardiomyopathy

Hypertrophic cardiomyopathy (HCM) is a genetic disease caused by mutations in contractile sarcomeric proteins that result in abnormal thickening of ventricular heart muscle, particularly the septum that separates that left and right ventricles (Figure 1.1) [1-6]. HCM can affect as many as 1/200 people, making it the most common genetic cardiomyopathy in the general population, as well as the most common cause of sudden cardiac death (SCD) [1, 7-9]. HCM is caused by rare genetic mutations in sarcomeric proteins, with the most common mutations found in *MYBPC3*

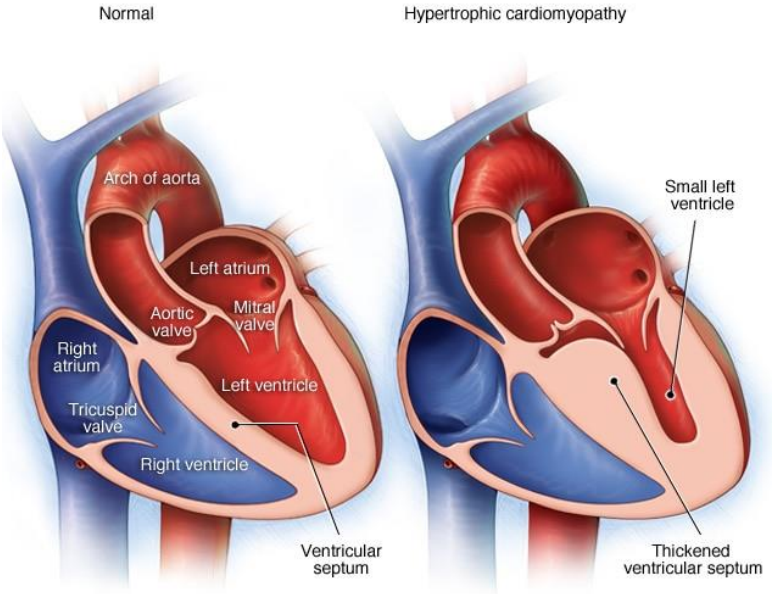

Figure 1.1 Healthy heart (left) and HCM heart (right).

(myosin binding protein C3) and *MYH7* (β-myosin heavy chain) genes [7]. These mutations accounts for ~50% of all cases of HCM.

Hypertrophic Obstructive Cardiomyopathy (HOCM) affects approximately 70% of patients with HCM [10] and is clinically defined as cardiac hypertrophy that is unexplained by loading conditions and includes the following complications: >13 mm left ventricular wall thickness, left ventricular outflow tract obstruction (LVOTO, non-dilated left ventricle), normal or increased ejection fraction, atrial or ventricular arrhythmias, heart failure, and/or SCD [1, 7, 11-14]. Atrial fibrillation (AF) occurs in roughly 1/5 HCM patients, a condition associated with thromboembolism. Myocardial fibrosis is a pathological hallmark of the disease, believed to be a key mechanism in adverse outcomes [15, 16]. HCM symptoms include shortness of breath or labored breathing (dyspnea), chest pain (especially during exercise), non-exertional and exertional angina, fatigue, and impaired consciousness including light-headedness, near-syncope, and syncope [17-20]. HCM is not an age-discriminant disease, as onset can occur during either childhood or adulthood [21, 22]. SDC occurs predominantly in adolescents and young adults, and as a result, current guidelines suggest HCM screening after 12-15 years of age [23].

1.2 Current Treatment Options for Hypertrophic Cardiomyopathy

Heart transplants are not readily available to all patients due to donor shortage, immune system compatibility, and so on. Because of this, pharmaceutical drugs are used to alleviate symptoms. Beta blockers are used to increase ventricular diastolic filling and promote relaxation of the heart muscle [21, 24]. Calcium channel blockers, such as Verapamil, augment ventricular diastolic filling and relaxation [25-28]. Finally, sodium channel blockers, used in combination with beta blockers, are negative inotropes used to weaken the force of ventricular contractions [29-31]. When medication alone is not sufficient to relieve symptoms, the current gold standard, septal myectomy, is performed [32]. Cardiothoracic surgeons perform the surgery by entering through the aortic opening and removing extra muscle tissue via resection using a scalpel. While this procedure has a high success rate with hopeful long term results [32-34], many patients are poor surgical candidates and require another, less invasive, treatment option. In these cases, cardiologists use the alcohol septal ablation (ASA) technique (Figure 1.2) [35]. Briefly, local anesthetic is applied to the skin of the groin area and an incision is made to allow a small catheter to be inserted into an artery or vein. The catheter is then threaded through the blood vessels all the way to heart using angiography or echocardiography to ensure the catheter is in the correct place. Finally, 1-4

mL of pure alcohol is released into a septal perforator (artery) to destroy part of the septal muscle via necrosis [36, 37]. The dead myocardium is removed from the body via phagocytosis. When given the option between surgical myectomy and ASA, most patients prefer ASA because of the lack of surgical incision, shorter recovery period, and lesser amount of pain [38].

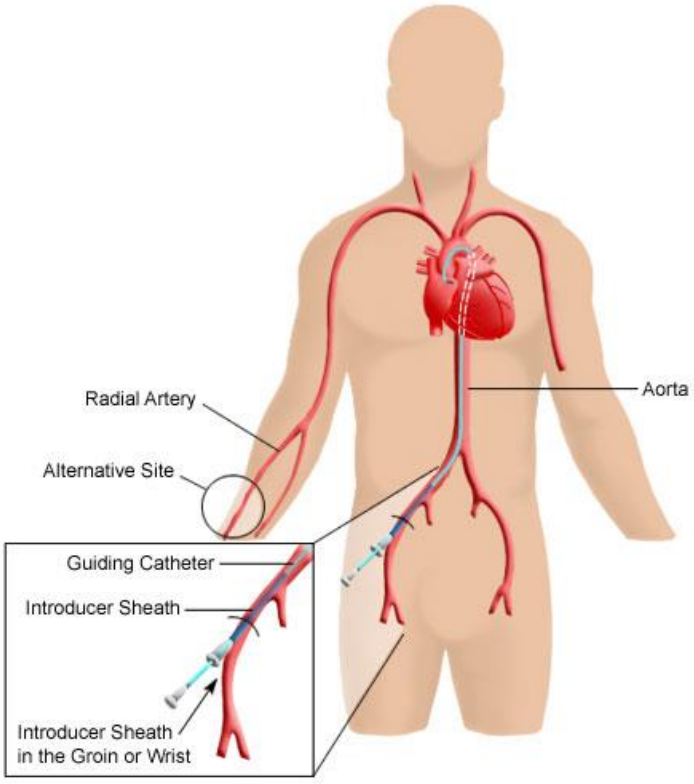

Figure 1.2. Schematic view of alcohol septal ablation (ASA).

1.3 The Problem with Alcohol Septal Ablation

Although ASA is a relatively common procedure for non-surgical patients, it has many downfalls. Chest pain during the procedure occurs in nearly every case but is treated through IV narcotics. Long-term complications are also relatively common, including atrioventricular block, ventricular fibrillation/tachycardia, left bundle branch block, or complete heart block [37, 39-43]. The most common of these complications is atrioventricular block, which is also a symptom of patients of all ages with HCM [44-48]. These complications result in the need of permanent pacemakers in 9-20% of cases with a periprocedural mortality rate of ~2% [49-51]. New intraventricular conduction defects (IVCDs) can be detected in 62% of patients following ASA [52]. The most alarming complication, however, is considerable myocardial necrosis due to lack of control of alcohol localization following injection [53-56]. The alcohol injected into the heart during the procedure is successful in killing the excess tissue, but in doing so damages an indiscriminate amount of healthy heart tissue as well. Overall, the current HCM treatments lack in either effectiveness or success rate considering the host of adverse responses that are often expected during or after these procedures. The ideal therapy is a minimally invasive, localized treatment specifically targeted to the diseased area to destroy the obstructive tissue and reduce the risk of both long- and short-term post-

procedure complications. In other words, an alternative septal ablation approach, which provides a controllable drug delivery to ensure accurate local ablation to shrink the extra septal tissue and hence mitigate the left ventricular outflow tract obstruction (LVOTO).

1.4 Existing Research for the Treatment of Hypertrophic Cardiomyopathy and the Potential Use of Nanotechnology

1.4.1 Ongoing Research for the Treatment of Hypertrophic Cardiomyopathy

Many different treatment options have been explored as alternatives to ASA. The use of cyanoacrylate (glue) in human patients has been used as an alternative treatment option in Turkey. To perform glue septal ablation, surgeons cannulated a left coronary ostium with a guiding catheter. The septal branch (septal perforator) was then cannulated with an additional catheter, followed by a microcatheter that released the cyanoacrylate mixture [10, 57]. Immediate polymerization of the cyanoacrylate of the glue was shown to prevent backflow. Okutucu and Oto *et al* noted that each patient that underwent glue septal ablation had a reduction in left ventricular outflow gradient and in septal size. No significant

complications occurred during surgery and up to 6 months after surgery; however, long-term efficacy is not known.

RNA trans-splicing and gene replacement strategies have also been explored as a treatment option for HCM [58-61]. Mearini *et al* utilized adeno-associated viruses (AAV) to carry pre-trans-splicing molecules (PTMs) carrying the wild-type (WT) *Mybpc3* cDNA sequence [58]. Following delivery, repaired cMyBP-C protein was detected in the sarcomere of cardiomyocytes, hinting at gene repair. Genetic correction of HCM has also been accomplished through the use of CRISPR/Cas9 gene editing [62-65] in which cardiomyocytes displayed normal electrophysiological properties and depletion of cardiac hypertrophy following CRISPR correction.

The use of microRNAs (miRNAs) as a potential treatment option has also been investigated. Researchers have synthesized miRNA-duplexes, which act as miRNA mimics, that include mature miRNA sequences and the complementary strand to deliver to the malfunctioning native miRNAs [66-68]. Targeting of the miRNA-duplexes has been accomplished through lenti-, adeno-, and adeno-associated viruses has been successful in targeted-delivery of the complexes [66-69]. There have also been several *in vivo* studies that have successfully inhibited cardiac hypertrophy and associated fibrosis [70-72]. Unfortunately, the uptake of miRNA-mimics may result in the overexpression of miRNA in otherwise healthy cells, which may

worsen the condition. Therefore, nanotherapies, including the use of nanoparticles, are an important route to consider to improve miRNA targeting [66].

Particularly of interest, recently, Doxorubicin has been considered as a potential treatment option for HCM. Although, in cancer patients, Doxorubicin has induced cardiomyopathy, it has also been shown to reduce the size of the septal tissue in pigs with HCM [73, 74]. Although the mechanism of Doxorubicin-ablation is controversial due to its toxicity, it proves to be a promising avenue to the future treatment of symptomatic HCM. Cardiac toxicity is thought to be mechanism of Doxorubicin only after repeat exposure, not by a single dosage [73]. Christiansen *et al* showed that, after Doxorubicin injection, there was macroscopic dilatation and tissue reorganization, showing that Doxorubicin was responsible for the clearance of unwanted cardiac tissue.

1.4.2 The Use of Nanoparticles to Treat Heart Diseases

Nanoparticles and microparticles have been used to treat heart diseases, such as atherosclerosis and ischemic heart failure for many years, particularly PLGA copolymer particles [75-84]. Additionally, liposomal formulations of Doxorubicin have been FDA-approved since the mid-1990s, particularly the treat inflammatory diseases of the heart [76].

Nanoparticles act as drug delivery systems and even as theranostic tools to treat and diagnose cardiac diseases. Drug-eluting stents have been used with Paclitaxel- or Doxorubicin-loaded particles to treat arterial stenosis [81]. Paclitaxel-loaded NPs have been shown to prevent re-stenosis of the artery. It stands to reason, then, that Doxorubicin, Paclitaxel's predecessor, may also be important in the use of tissue clearance, particularly septal tissue shrinkage.

1.5 Research Goals and Specific Aims

To overcome ASA limitations, our long-term goal is to design a new nanoparticle-mediated drug delivery system to replace the pure alcohol in ASA and achieve a controllable, localized septal tissue shrinkage and a safe ablation. The hypothesis is that the delivery of the novel Doxorubicin-loaded, collagenase-coated, degradable nanoparticles (NPs) will enable a breakdown of the fibrotic network in HCM tissue and allow an efficient localized Doxorubicin-induced killing of the hypertrophic cardiomyocytes, and hence shrink the overgrown HCM septal tissue. Three Aims will be pursued to develop this novel treatment approach. Aim 1 (Chapter 2): Perform ultrastructural and mechanical studies to determine the structural-functional relationship in healthy and diseased (HCM) tissues. Aim 2

(Chapter 3): Develop a novel drug-loaded, degradable nanoparticle system as an ablation means to treat abnormal hypertrophic septal muscle growth. Aim 3 (Chapter 4): Perform *ex vivo* studies to determine the localization ability of the collagenase-coated, drug-loaded nanoparticle system as well as the spatial distribution of nanoparticles compared to the unlocalized ASA technique.

As the current non-surgical treatment option for HCM, ASA is an unlocalized procedure resulting in uncontrollable, excessive myocardial death. As a major innovation, we hypothesize that the delivery of novel Doxorubicin-loaded, collagenase-coated, degradable nanoparticles will enable a breakdown of the fibrotic network in HCM tissue and allow an efficient localized Doxorubicin-induced killing of the hypertrophic cardiomyocytes, and hence shrink the overgrown HCM septal tissue. The proposed NP system shows promise because of the controlled delivery and release of cell-killing Doxorubicin, as well as targeting the fibrotic ECM that is connected to the basement membrane of hypertrophic cells [85, 86]. Using an *ex vivo* porcine heart model to assess the degree of localized delivery of the NPs and compare with the unlocalized ASA alcohol delivery technique is also a new effort important for future translational application.

CHAPTER 2

Ultrastructural and Mechanical Characterization of Human Healthy and Hypertrophic Cardiac Septal Tissues

Abstract

Introduction. Hypertrophic cardiomyopathy can be microscopically assessed and diagnosed by large cell size of the hypertrophic cardiomyocytes and disarray of those cells, as well as a fibrotic microenvironment. The extent of cell hypertrophy and fibrosis can directly impact the mechanical behavior of human cardiac septal tissues. In this chapter, we performed thorough ultrastructural and biomechanical characterizations on human septal tissues in both healthy condition and hypertrophic condition.

Methods and Results. Histological assessment using Masson's Trichrome staining revealed a large amount of collagenous fibrosis with a lack of directionality associated with disarrayed myocytes in HCM tissues when compared to healthy tissues. Passive uniaxial mechanical testing, shear mechanical testing, and biaxial mechanical testing were performed on healthy and HCM septal tissues. Uniaxial mechanical testing revealed larger stress decay and strain in HCM tissues, as well as almost linear stress-strain behavior. On the other hand, healthy septal tissues were more viscoelastic, allowing for a greater failure load.

Conclusion. The amount of myocardial disarray as well as the fibrotic environment of HCM have a direct result on the biomechanical properties

of the cardiac septum. HCM exhibited much stiffer behavior than healthy septal tissues in most mechanical testing results. However, contrary to previous results, HCM tissues underwent more strain than healthy septal tissues when applied under the same conditions.

1. Introduction

Hypertrophic cardiomyopathy (HCM) is a genetic disease of the sarcomere that results in overgrowth of the left ventricular septum [5, 17, 87, 88]. This overgrowth often causes mitral valve regurgitation and additional stress on the heart [89, 90]. A fibrotic collagenous microenvironment is associated with HCM due to this altered stress condition [91, 92]. Hypertrophy of the cells and the fibrotic environment contribute to the abnormal biomechanical properties of the septal tissues, and the extent of hypertrophy and fibrosis result in the regional impairment of the septum and left ventricle. Additionally, previous literature has shown that the circumferential myocardial shortening of ventricular muscle during contraction often occurs and is directly involved in the preservation of left ventricular systolic performance in HCM [93]. Reduced left ventricular strain, due to the thickening of the wall, has also associated with poor cardiac outcomes, which consequently result in heart failure and mortality [94].

The genetic background of HCM is well understood, but the ultrastructure and mechanics of HCM tissues are poorly defined. To study the effects of the cardiomyocyte hypertrophy and altered ECM microenvironment on the biomechanical properties of human cardiac septum, histology and biomechanical testing were performed. These

ultrastructural and mechanical assessments will allow us to determine the structural-functional relationship of the HCM septal tissues. The thorough understanding of the abnormalities in cardiomyocyte hypertrophy, disarray, and fibrotic collagen content/ultrastructure will build a strong foundation for further exploring treatment options for HCM.

2. Materials and Methods

2.1 Materials

Hypertrophic septal samples were obtained by way of surgical resection from 8 patients at the University of Texas Southwestern Medical Center (IRB STU 082017-072). Patients include both male and female and range in age from 19 years to 71 years. Seven of the patients suffered from hypertension, and other co-morbidities include coronary heart disease and high cholesterol. Most patients also presented with mild to moderate mitral valve regurgitation and septal thicknesses ranging from 1.7 cm to 3.2 cm. Additionally, all patients suffered from exertional dyspnea, and 4 patients suffered from non-exertional or exertional angina. Healthy human septal tissues were obtained from a tissue bank under the same IRB protocol.

For the HCM tissue, the septal samples were retrieved immediately after surgery and were placed in cardioplegia solution during transport to

the University of Texas at Arlington. Upon arrival, samples were examined to determine orientation. In this study, the longitudinal direction (LD) is determined as the axis that follows along the length of the trabeculae carneae and the cross-sectional direction (CD) is defined as the axis transverse to the trabeculae.

Septal tissues were then dissected for uniaxial tension testing, shear testing, and biaxial testing. Samples prepared for uniaxial testing had dimensions of ~15 mm (LD) x 10 mm (CD) x 3 mm (t), with the longest dimension aligned with the LD. All samples were further trimmed to achieve a dog-bone shape and 5 mm width. Dimensions of 3 mm x 3 mm x 3mm were used for shear testing. For biaxial mechanical testing, samples were dissected into square shapes, with dimensions of 10 mm (LD) x 10 mm (CD) x 3 mm (t). The remaining parts of the non-tested samples were used for histological evaluation. It should be noted that not all samples from this study were large enough for mechanical testing, and, therefore, those small size samples were only used for histological evaluation.

2.2 Methods

Microstructural analysis was performed on each patient sample after histological staining with Masson's Trichrome. The cell and fiber alignment

of the HCM tissue was investigated. Mechanical tests were completed within 4 hours of surgery to produce data from fresh tissue, and all the mechanical tests were performed in 1X Phosphate Buffered Saline (PBS) bath.

2.2.1 Light Microscopy and Microstructural Analysis

All samples were fixed in 10% neutral buffered formalin for 24 hours and were processed through a standard histological preparation protocol, including alcohol-dehydration, xylene-clearance, and paraffin-embedment. Sections were cut (5 μm) and a standard Masson's Trichrome staining protocol was performed. The Masson's Trichrome protocol stained heart muscle red and collagen blue. Histological images were taken under bright light field sing a Nikon Eclipse Ti Series Microscope (Nikon).

2.2.2 Uniaxial Tension Test and Characterizations of Tissue Viscoelasticity

Longitudinally oriented tissue samples were mounted on the TestResources Universal Testing Machine (Shakopee, MN, Figure 2.1) and the following testing protocols were completed: (1) Stress Relaxation: HCM (n=3) and healthy (n=3) samples were loaded to 100g and the achieved

strain was kept constant while recording the stress decay up to 15 minutes. (2) Creep: HCM (n=3) and healthy (n=3) samples were loaded to 100g and kept at this constant load while deformation was continuously monitored up to 15 minutes. (3) Tissue stress-strain behavior up to failure: HCM (n=3) and healthy (n=3) samples were loaded until failure (tissue breakage). Each sample was pulled at a rate of 0.5 mm/s.

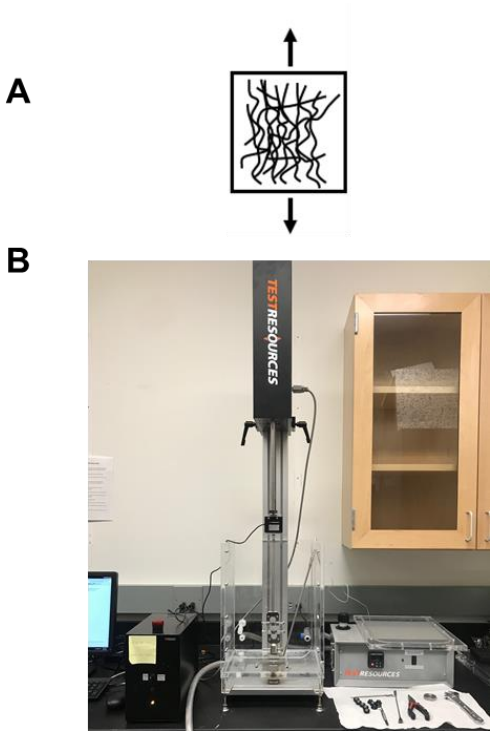

Figure 2.1 TestResources Universal Testing machine used for uniaxial and simple shear mechanical testing.

2.2.3 Simple Shear Test

Simple shear testing (Healthy: n=3; HCM: n=3) was performed to assess shearing property of the septal tissues. 3 mm x 3 mm x 3 mm cubed septal samples were mounted onto custom-built steel shear plates with minimal cyanoacrylate. The shear direction is along the longitudinal direction of the septal tissue. The shear plates were then mounted on the TestResources Universal Testing Machine. The samples were subjected to positive and negative shear up to 50% strain with a loading rate of 0.02 mms^{-1}.

2.2.4 Biaxial Mechanical Test

Septal tissue samples were dissected into 10 mm x 10 mm x 3 mm squares (Figure 2.2 A). Following dissection, samples (Healthy: n=3; HCM: n=6) were mounted to a custom-built biaxial mechanical testing system (Figure 2.2 B) using eight 000 polyester sutures with 16 stainless steel hooks in a 1X PBS bath. Samples were tested after 10 preconditioning cycles. After preconditioning, the equibiaxial tension protocol of T_{LD}:T_{CD} = 30:30 N/m was performed to capture the biaxial behavior. All the testing was performed with a 0.5 g tare load applied as a prerequisite for the software load control protocol, and the marker dimensions at 0.5 g tare load

were used as the reference status of biaxial mechanical testing. The stress-stretch curves were then obtained (Figure 2.8 B,C).

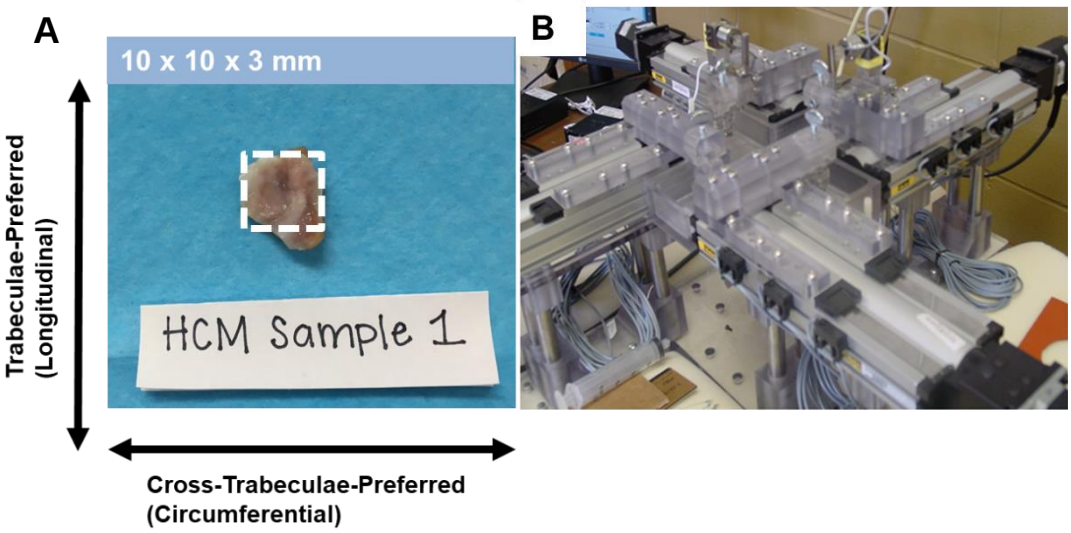

Figure 2.2 A) Dissected septal tissue cut into a square shape for biaxial mechanical testing. B) Custom-built biaxial mechanical testing machine.

2.3 Data Analysis

2.3.1 Cell Size and ECM Content

Brightfield light microscopic images of the Masson's Trichrome slides were taken using a Nikon Eclipse Ti Series Microscope. Heart muscle cells were identified by their red color and collagen content was identified by its blue color. The size of the hypertrophied cells was quantified using Fiji

particle image analysis with ImageJ software (Rasband, W.S., ImageJ, U. S. NIH, Bethesda, Maryland, USA, https://imagej.nih.gov/ij/, 1997-2018).

2.3.2 Cell and Collagen Fiber Orientation

To analyze the cell and collagen fiber distribution, the Masson's Trichrome images were converted to 8-bit gray scale images and later subjected to thresholding to capture the cell morphology or the ECM morphology using ImageJ protocols. Area occupied by cells and average cell size were quantified using ImageJ particle analyses. Using the OrientationJ plugin in ImageJ, we were able to determine cell and collagen fiber orientation distribution from -90 degrees to 90 degrees (Figure 3.2) [95].

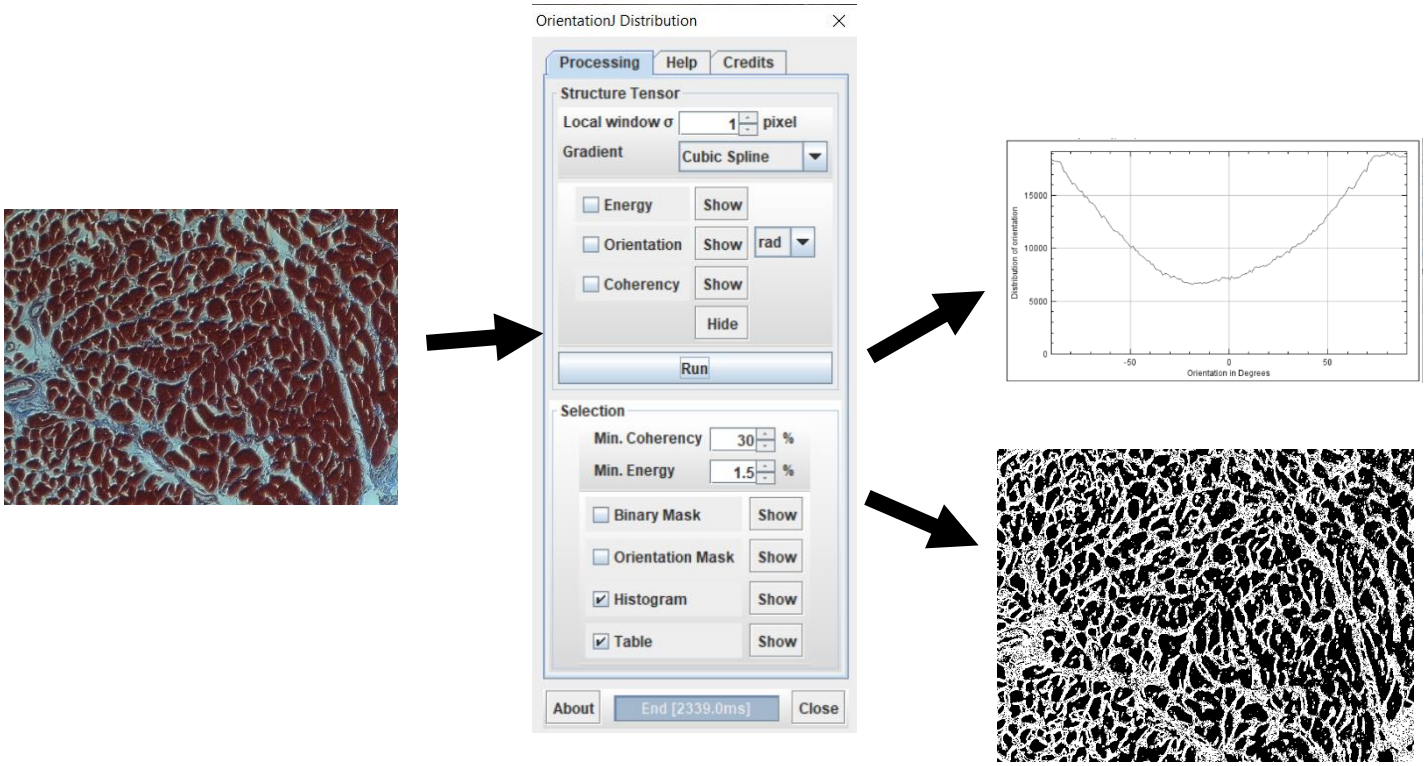

Figure 2.3 Representative layout of OrientationJ for cell and fiber distribution analysis.
Process for analyzing the cell and fiber distribution angles in ImageJ. (A) Mason's trichrome histology; (B) Settings used for OrientationJ analysis; (C) Orientation mask produced from OrientationJ; (D) Cell and fiber distribution result reported by OrientationJ.

2.3.3 Estimation of Stress and Strain

Engineering stresses in healthy (σ_H) and HCM (σ_{HCM}) tissues are calculated by normalizing the applied force (f) to the initial cross-sectional area (A) of the sample. Strains (ε_H and ε_{HCM}) are calculated by normalizing the amount of deformation to the initial dimension.

$$\sigma_H = f_H / A_H, \ \sigma_{HCM} = f_{HCM} / A_{HCM} \qquad \textit{(Eq. 2.1)}$$

$$\varepsilon_H = \Delta X_H / X_H, \ \varepsilon_{HCM} = \Delta X_{HCM} / X_{HCM} \qquad \textit{(Eq. 2.2)}$$

Where ΔX_H, ΔX_{HCM} represent the amount of deformation and X_H, X_{HCM} represent the initial length of the sample.

2.3.4 Simple Shear Tests

Shear stress (τ) is the normalization of the shear force (f) to the cross-sectional area A (for our sample $A = L^2$).

$$\tau = f/A = f / L^2 \qquad \textit{(Eq. 2.3)}$$

The amount of shear strain (γ) is calculated by normalizing the shear plate displacement to the sample thickness L.

$$\gamma = \Delta L / L \qquad \textit{(Eq. 2.4)}$$

where ΔL represents shear plate displacement and L represents the sample thickness.

2.3.5 Statistical Analyses

All values are reported as the mean ± standard deviation (SD), where a p-value less than 0.05 was considered as statistically significant. One-way analysis of variances (ANOVA) was performed along with Tukey HSD *post hoc* test to quantify the statistical significance of the healthy and HCM septal tissues. All statistical analyses were conducted in RStudio (R Foundation for Statistical Computing, Vienna, Austria).

3. Results

3.1 Microstructural Analysis

Average cell area and diameter (Figure 2.4 C) was quantified from histological images of human healthy (Figure 2.4 A) and HCM hearts (Figure 2.4 B). Healthy heart cell area was, on average, 1148 ± 1071 μm^2, with an average diameter of 19 ± 6.5 μm. On the other hand, HCM cells were much larger, with a mean area of 3536 ± 2142 μm^2 and an average diameter of 31 ± 11.5 μm. Previous literature confirms our results that HCM

cell size is larger than healthy cells [96, 97]. To further examine myocardial and collagen disarray, we observed the cell and collagen fiber distribution.

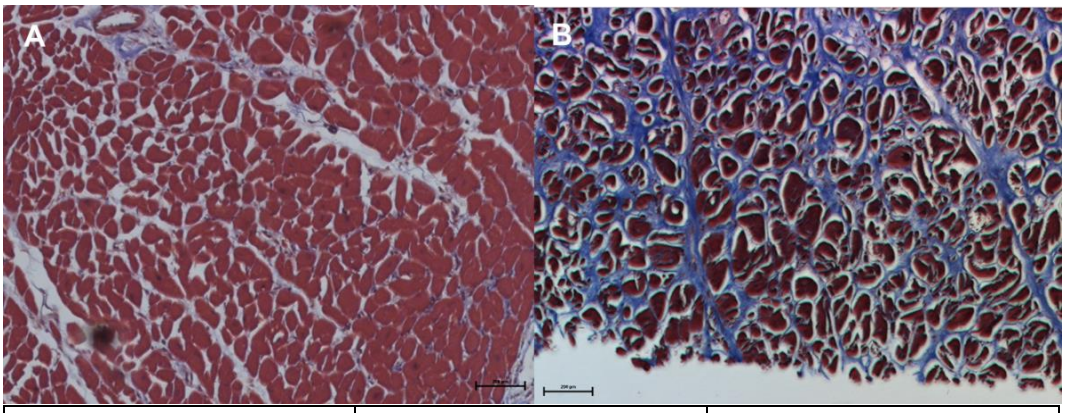

C	Healthy	HCM
Area (μm^2)	1148 ± 1071	19 ± 6.5
Diameter (μm)	3536 ± 2142	31 ± 11.5

Figure 2.4 Masson's Trichrome images of human healthy (A) and HCM (B) septal tissues. (C) Average area and diameter of healthy and HCM septal tissues.

Cell and collagen fiber distribution was quantified from histological images of in-plane sections. The cell and fiber distribution from -90 degree to +90 degree was then plotted in Figure 2.5. The fiber distribution curves showed that fiber alignment was different between the groups. These quantitative results were consistent with the histological observation,

showing that healthy cells and collagen fibers had a more aligned distribution, while the HCM cells and collagen fibers had a more random (disarrayed) distribution.

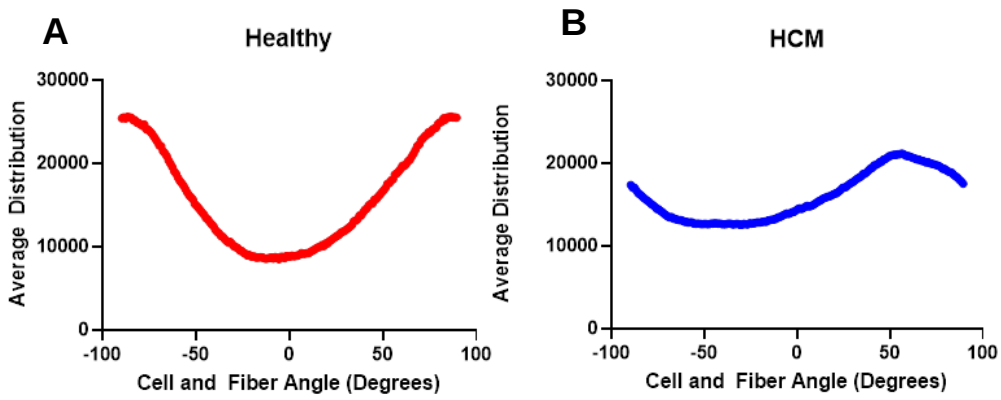

Figure 2.5 A) Healthy septal tissue's cell and collagen fiber alignment histogram. B) HCM cell and collagen fiber alignment histogram.

3.2 Viscoelastic Properties, Failure Stress-Strain Curves, and Simple Shear Behavior

3.2.1 Stress Relaxation.

Stress relaxation is defined as decrease in stress of a material when a constant strain is applied and maintained [98]. Healthy septal tissues exhibited a stress decay similar to most soft tissues, 57 ± 6.3%. On the other hand, HCM septal tissues exhibited a much larger stress decay, 68 ± 11%. Stress decay was greater in HCM tissues due to the abundance of the fibrotic collagen matrix. Interfibrillar sliding of collagen fibrils allows for greater stress decay [99].

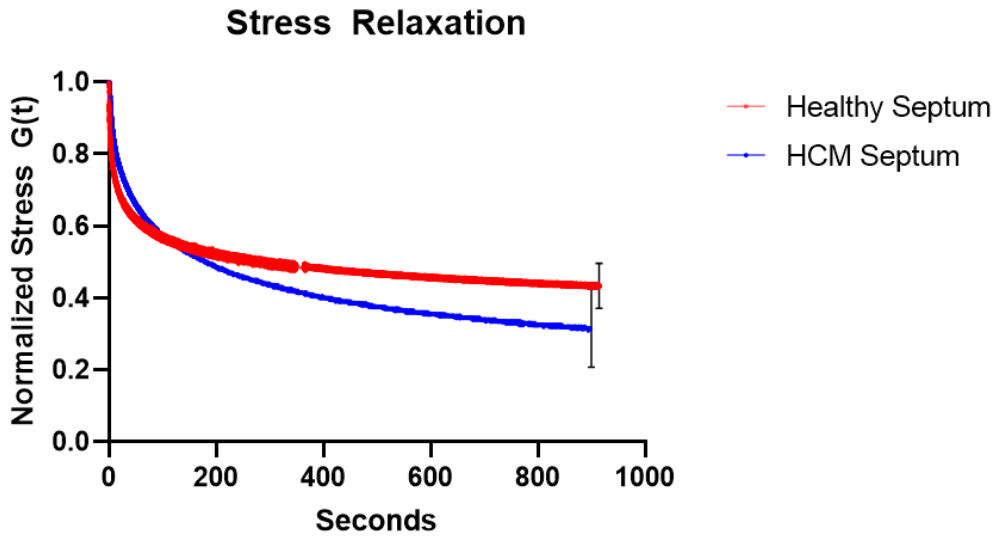

Figure 2.6 Stress Relaxation- Average stress relaxation data (n=3/group) for human healthy (red) and hypertrophic (blue) cardiac septal tissue. For healthy tissue, approximately 55% stress decay was observed. For HCM tissue, approximately 70% stress decay was observed.

3.2.2 Creep.

Creep is defined as the deformation of a material over time when the sample is subjected to a constant load [100]. Both healthy septal tissues and HCM septal tissues showed a small amount of creep over time. The final creep amount at 15 minutes reached 9.1 ± 1.0% for healthy septal tissues and 9.8 ± 4.2% HCM septal tissues. Although not statistically significant, HCM septal tissues showed a creep amount that is slightly larger than the healthy septal tissues. More samples are needed to verify this trend. If verified, this can likely be attributed to more abundant and more disarrayed fibrotic collagen fibers that is associated with HCM.

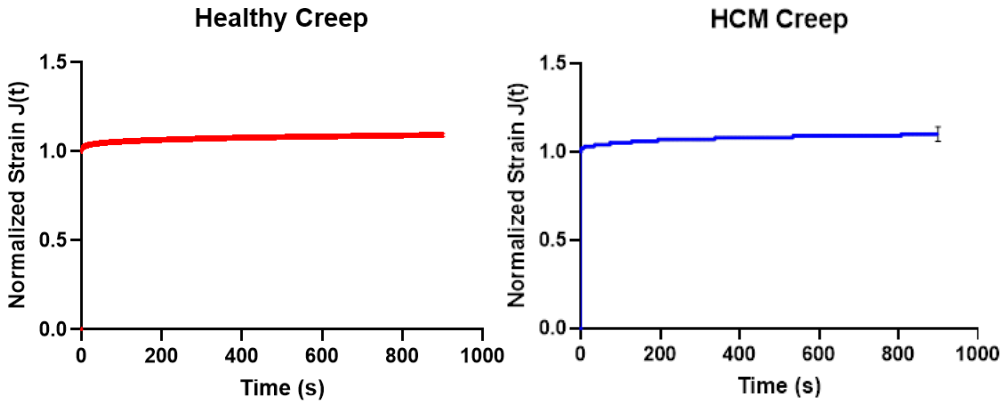

Figure 2.7 Average creep data (n=3/group) for human healthy (red) and hypertrophic (blue) cardiac septal tissue. Average strain for healthy tissue was 8.6 ± 0.042. Average strain for HCM tissue was 10% ± 0.0056.

3.2.3 Stress-Strain Behavior up to Tissue Failure.

Prior to extension, ten preconditioning cycles were performed. The averaged uniaxial stress-strain curve (Figure 2.8) of the healthy septal tissues showed a very typical nonlinear concave upward stress-strain relation. The HCM tissues, however, showed a stress-strain trend that was much less nonlinear. The HCM septal tissues has an initial modulus that is higher than healthy septal tissues (healthy: 311 ± 284 kPa vs HCM: -263 ± 57 kPa), most likely due to the abundant fibrotic collagen associated with HCM. Very interestingly, we found that the healthy septal tissues had much higher mechanical strength than the HCM septal tissues, demonstrated by the failure stress (healthy: 2,561 ± 919 kPa vs HCM: 494 ± 206 kPa). In the high strain region, the healthy septal tissues were also stiffer than the HCM septal tissues, as shown by the maximum tensile modulus of the tissues. Overall, HCM septal tissues were stiffer at the initial phase of tissue loading, less nonlinear, less stiff in the linear region, and much weaker in mechanical strength. This is a very novel biomechanical finding of this disorganized, hypertrophic, and fibrotic heart muscle tissue.

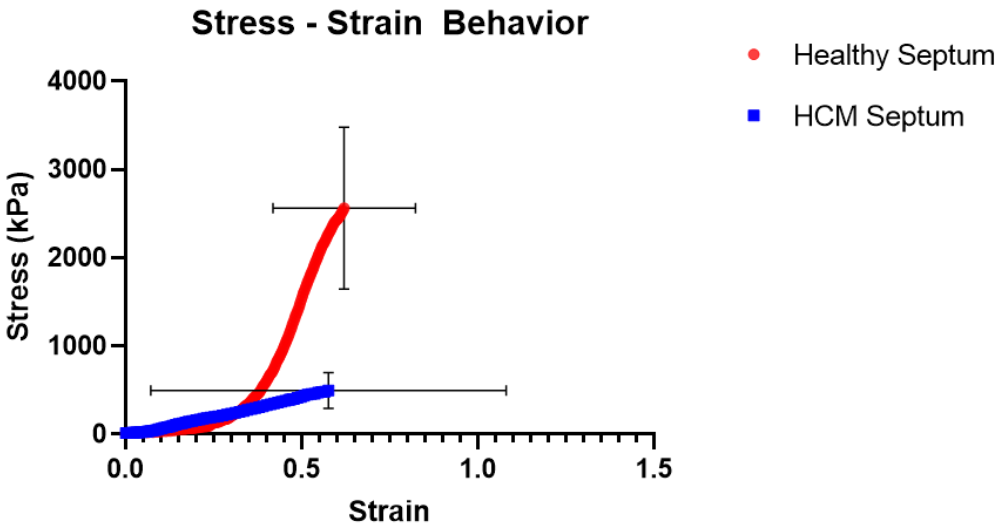

Figure 2.8 Average stress-strain behavior of healthy (red) and HCM (blue) cardiac septal tissues (n=3/group).

3.2.4 Simple Shear

Energy dissipation (hysteresis) is evident throughout cyclic shearing behavior, with both healthy and HCM tissues demonstrating a nonlinear shear behavior (Figure 2.9). The HCM septal tissues (blue) appear much stiffer with greater energy dissipation than the healthy septal tissues (red). The maximum shear modulus of the healthy septal tissues and HCM septal tissues were 100 ± 12 kPa and 250 ± 73 kPa, respectively.

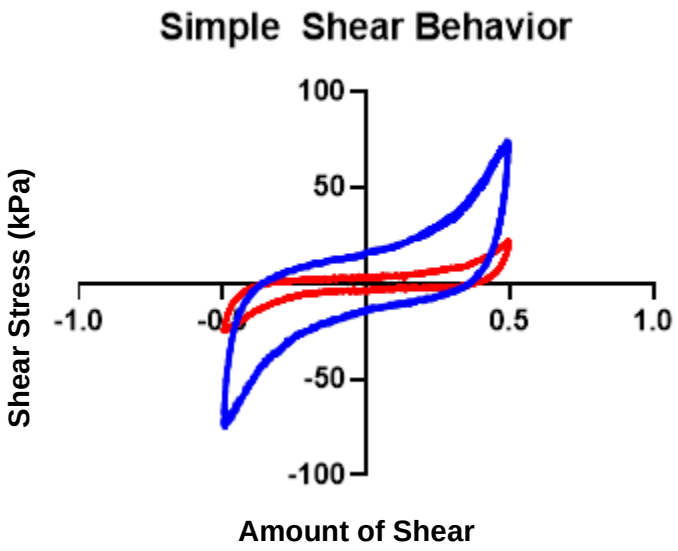

Figure 2.9 Demonstrating passive simple shear behavior of healthy (red) and HCM (blue) cardiac septal tissues at 50% shear (n=3/group).

3.3 Biaxial Mechanical Behavior

The biaxial mechanical stress-strain curves were shown in Figure 2.10. Healthy and HCM septal tissues possessed nonlinear, anisotropic mechanical responses. HCM septal tissues were found to be stiffer than the healthy septal tissues in the longitudinal direction (Figure 2.10), which was consistent with the uniaxial stress-strain behavior in the initial region of uniaxial stress-strain curve (Figure 2.8). In the longitudinal direction, the extensibility of HCM septal tissues was 1.7 ± 1.6% , while the extensibility of healthy septal tissues was 6.4 ± 0.25%. The circumferential direction appears similar between both groups with 8.0 ± 3.4% stretch for healthy tissues and 7.5 ±3.7% stretch for HCM tissues.

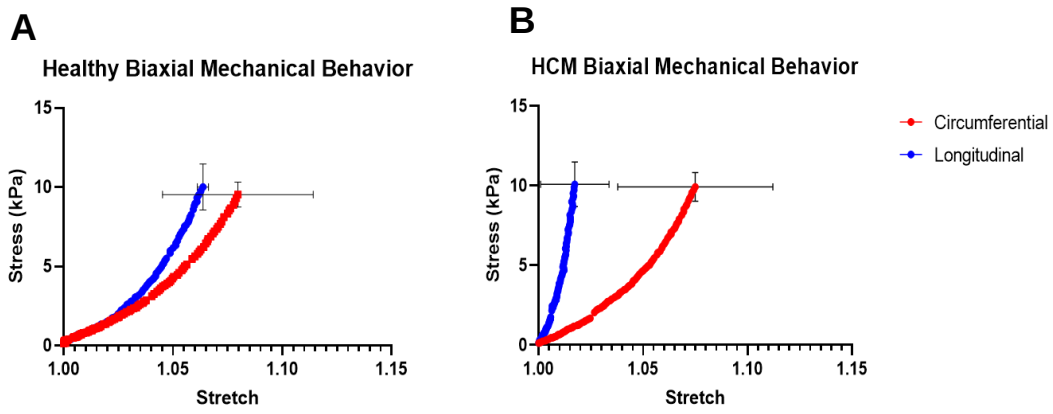

Figure 2.10 A) Average biaxial mechanical behavior of healthy human septal tissue (n=3). B) Average biaxial mechanical behavior of human HCM septal tissue (n=6).

4. Discussion

Septal tissues were observed via Masson's Trichrome histological staining (Figure 2.4 A,B). Larger cell content and bigger cell size (area percentage: 3536 ± 2142 μm^2 and cell diameter: 31 ± 11.5 μm) was observed in HCM tissues compared to healthy tissues (area percentage: 1148 ± 1071 μm^2 and cell diameter: 19 ± 6.5 μm) (Figure 2.4 C). Moreover, HCM tissues exhibited larger areas of collagen (fibrosis). The cell and collagen fiber distribution curves (Figure 2.5) demonstrated HCM were less aligned and arranged more randomly.

This study has identified non-linear, anisotropic, and viscoelastic mechanical behavior of human healthy and HCM cardiac septal tissues. This viscoelastic responses are typical characteristics of soft tissues due to the interaction between solid structures and hydrated ground substance [101]. The nonlinear, concave upward stress-strain curve of the healthy tissues are consistent with that of other soft tissues [101, 102]. All uniaxial extension tests were performed following 10 preconditioning cycles [101, 103-106]. Stress relaxation testing revealed that HCM tissues exhibit a much larger stress decay (68 ± 11%) than that of healthy septal tissues (57 ± 6.3%) (Figure 2.6), as well as other soft tissues [107]. Additionally, creep testing showed that the healthy septal tissues were slightly more resistant

to creep when compared to the HCM septal tissues (Figure 2.7). All stress relation and creep observations likely reflected the fact that HCM septal tissues had more disorganized fibrotic collagen fibers when compared with the healthy septal tissues.

Uniaxial tensile stress-strain curves up to failure revealed that healthy septal tissues were less stiff than healthy septal tissues in the initial loading region, but was much stiffer in the linear region and had a much higher mechanical strength that the HCM septal tissues (Figure 2.8). The healthy septal tissues really took an optimal soft tissue biomechanical behavior, in which a shallow toe region, and smooth transitional region, and a sharp rising linear regions has large tensile modulus and failure stress. On the other hand, the almost linear, large initial stiffness, low maximum stiffness, and low failure stress reflected faulty design, which apparently was the result of pathologically structural alterations due to HCM.

As the strain increased, the healthy septal tissues gradually recruited a collagen network that was more organized at ultrastructural level and well-integrated with heart muscle cells, and hence was able to achieve optimal nonlinear concave upward stress-strain curve shape, in which the recruited collagen fiber network provided a locking-up mechanism to protect the muscle fibers and avoid the tear and debonding. The poorly organized,

pathological compositions in HCM seemed to lose the benefit of native tissue design and hence exhibited an inferior mechanical behavior as described above. However, the abundant disorganized fibrotic collagen network in HCM septal tissues did increase the initial tensile modulus in uniaxial extension, as well as cause a stiffer behavior and a greater energy dissipation in simple shear.

5. Limitations

Due to the limited number of samples and the size of the samples received, not all samples could be used for mechanical testing. However, these results are still representative of the HCM population, and all samples were examined histologically. The disarray (cellular and ECM) found in HCM varies from patient-to-patient which may explain the larger margin of error in mechanical testing. Additionally, uniaxial mechanical testing was only measured along the longitudinal plane due to the small size of the samples received from surgery.

5. Conclusions

The over-expressed, disorganized, fibrotic ECM present in HCM plays a significant role in its abnormal mechanical properties. Large cell size and disarray of cells, along with a large amount of poorly organized collagen, had a great and direct effect on the mechanical properties of the HCM septal tissues. In this study, we thoroughly described the nonlinear, anisotropic, and viscoelastic mechanical behavior of human healthy septal tissues, as well as how the HCM septal tissues lost the optimal mechanical behavior due to poorly-organized, pathological compositions in HCM. The ultrastructural and biomechanical data we collected provide a strong foundation to understand tissue behavior of HCM septal tissues in relation to healthy septal tissues.

CHAPTER 3

Nanoparticle-Mediated Controlled Myocardial Drug Delivery: A New Treatment for Hypertrophic Cardiomyopathy

Abstract

Introduction. Hypertrophic cardiomyopathy is currently treated by either septal myectomy or alcohol septal ablation (ASA). Although it does not carry the risks involved in surgery, the ASA procedure has many faults. To combat these issues, we have designed a targeted nanoparticle (NP) drug delivery system and tested its efficacy *in vitro* using a 2D model.

Methods and Results. Nanoparticles were prepared using a standard double emulsion technique. HL1 cells were seeded onto collagen coated plates to mimic the fibrotic environment associated with HCM. Hypertrophy was induced in HL1 cardiomyocytes by stimulating them with endothelin-1 (ET-1). Following ET-1 treatment, cells were treated with various concentrations of collagenase coated, Doxorubicin-loaded PLGA (COL-PLGA-DOX) nanoparticles. COL-PLGA-DOX NPs killed hypertrophic cells at a rate like that of free, unlocalized Doxorubicin, proving the efficacy of our NPs.

Conclusion. COL-PLGA-DOX treatment killed hypertrophic cells at a similar rate of free, untargeted Doxorubicin. This study showed that our NP system can kill diseased cells *in vitro*. Future *in vivo* studies should be performed in an animal model to confirm the localization ability of the NPs to the diseased cardiac septum.

1. Introduction

Hypertrophic cardiomyopathy (HCM) is a genetic disease caused by mutations in contractile sarcomeric proteins that result in abnormal thickening of ventricular heart muscle. This condition most commonly affects the cardiac septum that separates that left and right ventricles [1, 12, 108-110]. HCM can affect up to 1/200 people, making it the most common genetic cardiomyopathy in the general population, as well as the most common cause of sudden cardiac death (SCD) [1, 7-9]. HCM is caused by rare genetic mutations in sarcomeric proteins with the most common mutations found in *MYBPC3* (myosin binding protein C3 gene) and *MYH7* (myosin heavy chain 7) genes [7].

HCM is cardiac hypertrophy that is unexplained by loading conditions, and patients often experience left ventricular wall thicker than 13 mm, left ventricular outflow tract obstruction (LVOTO, non-dilated left ventricle), normal or increased ejection fraction, atrial or ventricular arrhythmias, heart failure, and/or SCD [1, 7, 11-14]. HCM symptoms include shortness of breath or labored breathing (dyspnea), chest pain (especially during exercise), exertional angina, fatigue, and impaired consciousness including light-headedness, near-syncope, and syncope [17-20]. Onset of HCM can occur during either childhood or adulthood [21, 22]. SDC occurs predominantly in adolescents and young adults, and as a result, current

guidelines suggest HCM screening after 12-15 years of age [23]. Heart transplants are not readily available to all patients due to donor shortage and immune system compatibility issues. Additionally, most HCM cases do not require heart transplants, and depending on the severity of the disease, may be treated with pharmaceutical drugs such as beta blockers, calcium channel blockers, and sodium channel blockers.

When medication alone is not sufficient to relieve symptoms, the current gold standard, septal myectomy, is performed [32]. Cardiothoracic surgeons perform the surgery by entering through the aortic opening and removing extra muscle tissue via resection using a scalpel. While this procedure has a high success rate with hopeful long term results [32-34], many patients are poor surgical candidates and require a less invasive treatment option. In these cases, cardiologists use the alcohol septal ablation (ASA) technique**.** During the ASA procedure,1-4 mL of pure alcohol is released into a septal perforator (artery) into the septum to destroy part of the septal muscle via necrosis [36, 37]. The dead myocardium is removed from the body via phagocytosis.

However, ASA has many inadequacies that cannot be overlooked. The most common ailment resulting from ASA is complete heart block which can results in heart failure (HF). In several of these cases, there is a need

for permanent pacemakers. The most notable side effect of the ASA procedure is excessive myocardial death, which occurs when the unlocalized alcohol extends into the healthy myocardium and regions that are not part of the overgrown septum.

To avoid these issues in the future, we have designed a nanoparticle (NP) drug delivery system (Figure 3.1) that is localized to the fibrotic collagen of the diseased septum. Using a 2D culture model with hypertrophic HL1 cardiomyocytes seeded on a collagen coated plate (mimicking the fibrotic environment), we have tested the efficacy of this NP drug delivery system.

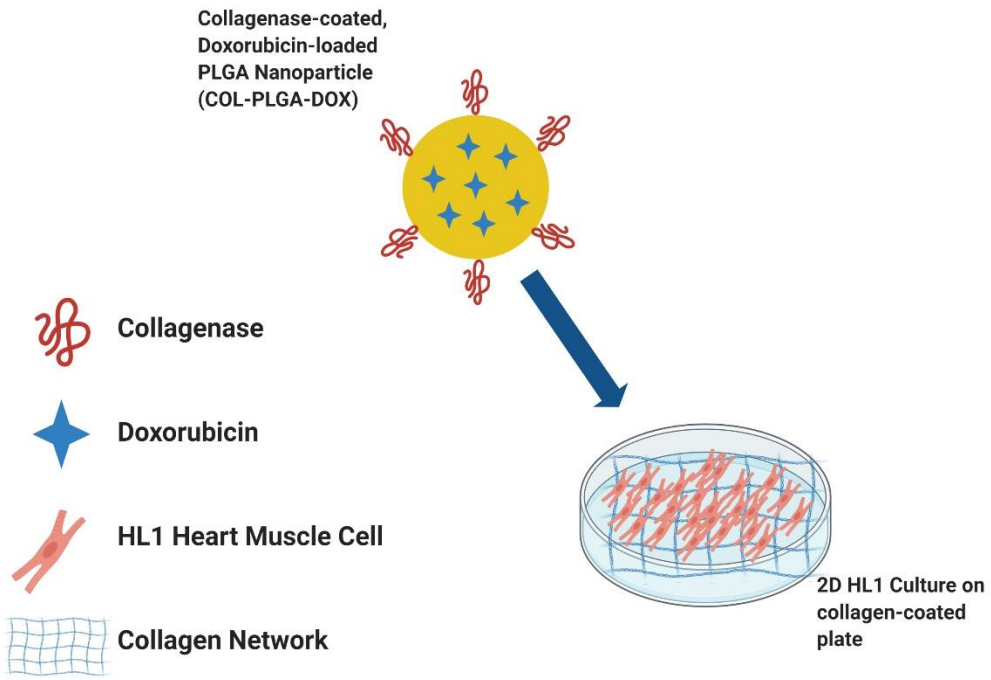

Figure 3.1 Schematic of experimental procedures with legend.

2. Experimental Section

2.1 Materials

Dimethyl sulfoxide (DMSO), dichloromethane (DCM), polyvinyl alcohol (PVA), and collagen coating solution were purchased from Millipore Sigma. Doxorubicin HCl (DOX) was purchased from Cayman Chemicals. Poly(lactide-co-glycolide) (PLGA 50:50) and PLGA-NHS (20-40 kDa) were purchased from PolySciTech® (Molecular weight of 25-35 kDa). Collagenase (COL) was purchased from Fisher Scientific. HL1 cardiomyocytes were obtained from Dr. Zui Pan (University of Texas at Arlington, College of Nursing and Health Innovation, Arlington, TX, USA).

2.2 Fabrication of COL-PLGA-DOX Nanoparticles

DOX-loaded PLGA NPs were prepared by a standard double emulsion process. Briefly, 100 mg of PLGA (90% PLGA 50:50, 10% PLGA-NHS) was dissolved in 3 mL DCM. PLGA-NHS was used to allow for conjugation of COL to the surface of the NPs (described at a later step). DOX was dissolved in 120 µL DMSO. Once PLGA was completely dissolved, the drug solution was added dropwise on a stir plate at room temperature. The resulting oil emulsion was then sonicated on ice for 3

minutes at 30 watts and was then added to 5% PVA on a stir plate at room temperature. This solution was then ultrasonicated at 25 amps. After overnight stirring at room temperature, the NPs were washed with deionized water and were collected by ultracentrifugation and lyophilization. Blank PLGA NPs were also fabricated using the same process as above, without the addition of DOX. Similarly, FITC-loaded NPs were fabricated, replacing the DOX step with FITC.

To conjugate COL to the surface of the DOX-loaded PLGA particles, 20 µg (per 10 mg of NPs) of COL were added to a NP solution in PBS (1 mg/mL). The solution was incubated overnight at 4°C. Following the incubation, the NPs were collected by ultracentrifugation at 15,000 rpm for 30 minutes. The supernatant was used to determine peptide conjugation efficiency. Pellets were resuspended in DI water and were lyophilized.

2.3 Characterization of Nanoparticles

Using a dynamic light scattering (DLS) technique, particle size and surface charges were measured using a ZetaPALS zeta potential analyzer (Brookhaven Instruments Inc.). The morphology of the particles was also analyzed using transmission electron microscopy (TEM, JOEL 1200EX). A drop of particle solution (2 mg/mL) was placed on a Formvar-coated 200-

mesh copper grid (Electron Microscopy Sciences,Hartfield, PA) at room temperature and allowed to air-dry followed by treatment with 0.1% uranyl acetate solution. The sample was then inserted into the TEM instrument for observation.

2.4 Collagenase Conjugation Efficiency and Collagen Degradation Studies

2.4.1 Collagenase Conjugation

Collagenase conjugation was confirmed by Fourier-transform infrared spectroscopy (FTIR).

2.4.2 Collagen Degradation

The effect of collagen degradation by collagenase was assessed both quantitatively and qualitatively as has been previously recorded in the literature [111]. Collagen was obtained from left ventricular heart muscle by decellularization with 1% sodium dodecyl sulfate (SDS). For quantitative determination, collagen degradation was carried out in 1X PBS (pH 7.4) using 1, 10, 25, 50, 100, and 200 U/mL of COL for 48 hours at 37°C. Furthermore, collagen degradation was carried out in 1X PBS (pH 7.4)

using COL-PLGA-DOX at 1, 50, 100, and 250 µg/mL for 48 hours at 37°C to assess collagen degradation qualitatively and quantitatively.

2.4.2.1 Enzymatic (Collagenase) Degradation of Collagen

Prior to the addition of collagenase, samples (n=3 per group) were lyophilized and their masses were recorded. COL was added at the previously mentioned concentrations and were incubated for 48 hours. Afterwards, the supernatant was removed, and the samples were freeze-dried again. The mass of the freeze-dried samples were then recorded. The mass lost due to collagenase degradation was assessed using the following formula: $M = [(M_0 – M_t) / M_0]*100$, where M_0 represents the initial mass of the samples, M_t represents the final mass, and M represents mass lost as a percentage.

2.4.2.2 COL-PLGA-DOX Degradation of Collagen

Collagen degradation was assessed visually and quantitatively by Masson's Trichrome staining. All samples were fixed in 4% paraformaldehyde and were embedded in paraffin. Sections were deparaffinized and rehydrated in distilled water on a glass slide. The slides

were added to preheated Bouin's Fluid for 60 minutes, followed by a 10-minute cooling period. The slides were rinsed again until fully clear and then stained with Weigert's Iron Hematoxylin for 5 minutes followed by rinsing. Beibrich Scarlet/Acid Fuchsin solution was applied to each slide for 15 minutes followed by rinsing. Phosphotungstic Acid solution was added for 15 minutes, until collagen was no longer red. Aniline Blue solution was added for 10 minutes followed by rinsing. Acetic Acid Solution (1%) was added to the slides for 5 minutes, followed by dehydration with alcohol, and clearance with xylene. To quantitatively assess the degree of collagen per 5 µm slice, we used the ImageJ thresholding feature.

2.5 Cytotoxicity Analysis of Nanoparticles

HL-1 Cardiomyocytes were seeded at a density of 20,000 cells/well in a 96-well plate coated with collagen to mimic the fibrotic environment of HCM. Cells were incubated overnight to facilitate cell attachment. The cells were then incubated with blank (non-drug loaded) PLGA NPs at the following concentrations: 10, 100, 250, 500, 1000 µg/mL. After 24-hour incubation, cell viability was measured using MTS cell viability assays (CellTiter 96®Aqueous One Solution Cell Proliferation Assay, Promega).

2.6 Cellular Uptake of Nanoparticles

Cell uptake of the PLGA NPs was determined by measuring the FITC-labeled PLGA NPs that were internalized by the cells. HL1 cardiomyocytes were seeded at a seeding density of 20,000 cells/well in a collagen-coated 96-well plate. After overnight attachment, the cells were incubated with the FITC-PLGA particles at concentrations of 50, 100, and 250 µg/mL at 37°C for 2 hours. Afterwards, cells were washed with sterile 1X PBS three times and were lysed using Triton X-100. To quantify the NPs internalized by the cells, the fluorescence intensity of FITC at wavelengths of λ_{ex} 495 nm and λ_{em} 519 nm was measured. The fluorescence intensity was normalized against the amount of total protein from cells per well using bicinchonic acid assay (BCA) as per the manufacturer's protocol (PierceTM BCA Protein Assay Kit, Thermo Scientific).

HL1 cell uptake of FITC-PLGA was also visualized by fluorescent imaging. HL1 cardiomyocytes were seeded at 30,000 cells/chamber on an 8-chamber microscope slide coated with collagen. After overnight attachment, HL1 cells were subjected to 50 µg/mL, 100 µg/mL, and 250 µg/mL of FITC-PLGA NPs for 2 hours. Then, cells were washed three times with 1X PBS followed by fixation for 30 minutes in 4% paraformaldehyde. To remove excess paraformaldehyde, the cells were washed once more.

The nuclei were stained with NucBlue (ThermoScientific). The cells were then observed under a fluorescent microscope (Cytoviva, Inc).

2.7 *In vitro* Hypertrophic Cell Death Studies

The *in vitro* killing efficiency of COL-PLGA-DOX NPs was determined by cytotoxicity assays. Briefly, HL1 cardiomyocytes were seeded at a seeding density of 20,000 cells per well on a collagen-coated 96 well plate and cultured overnight. Cells were seeded at a higher density due to the fragility (ease of dissociation from the plate and slower proliferation times) of the cells when seeded on collagen. The cells were treated with 1 µM of endothelin-1 (ET-1, FisherScientific) to induce hypertrophy of the cells and were cultured for 48 hours. Cells were then treated with 2.6 µg/mL (IC50) and 4.16 µg/mL (IC75) of free doxorubicin and the IC50 and IC75 NP equivalents based on the drug loading results. Untreated cells and cells treated with Triton-X served as the positive and negative controls, respectively. After 48 hours, cell death was determined by MTS assays (CellTiter 96®Aqueous One Solution Cell Proliferation Assay, Promega).

2.8 Statistical Analyses

All values are reported as the mean ± standard deviation (SD), where a p-value less than 0.05 was considered as statistically significant. Two-way analysis of variances (ANOVA) was performed along to quantify the statistical significance of the cytocompatibility, cell uptake, and *in vitro* killing assays. All statistical analyses were conducted in RStudio (R Foundation for Statistical Computing, Vienna, Austria).

3. Results

3.1 Nanoparticle Characteristics

The biodegradable PLGA nanoparticles were fabricated using a double emulsion technique. The PLGA-DOX and COL-PLGA-DOX NPs had a mean diameter of 203 ± 37.4 nm and 181 ± 40.0 nm, respectively (Figure 3.2 A). The zeta potentials of PLGA-DOX and COL-PLGA-DOX were -8.6 ± 1.6 mV and -8.5 ± 0.6 mV, respectively. TEM images revealed a spherical, smooth morphology for both NP groups (Figure 3.2 B). The drug (DOX) loading efficiency was determined to be ~70%. DOX release kinetics (Figure 3.2 C) revealed that, over a period of 14 days, ~60% of the drug was released, with a sharp increase in drug release within 2 days. The

higher drug release in the first two days is likely due to the low molecular weight of the PLGA which allows for a burst release of the drug.

A

Nanoparticle	Size (nm)	Zeta Potential
PLGA-DOX	203 ± 37.4	-8.6 ± 1.6
COL-PLGA_DOX	181 ± 40.0	-8.5 ± 0.6

B

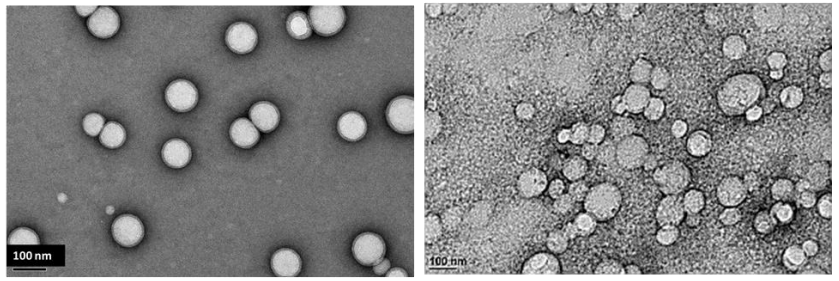

C

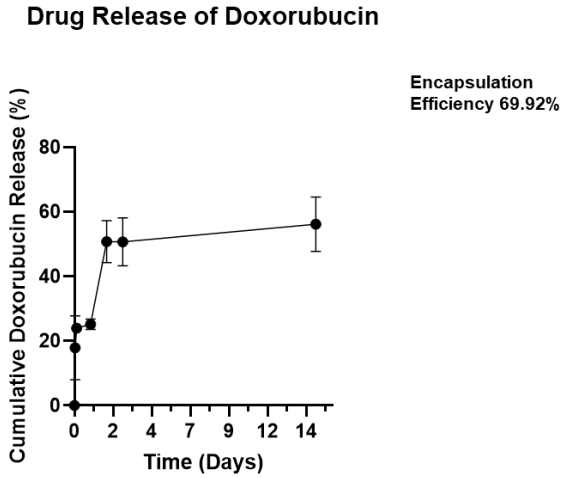

Figure 3.2 A) Average NP size and zeta potential. B) Representative TEM images of PLGA-DOX NPs (left) and COL-PLGA-DOX NPs (right). C) Drug release kinetics of Doxorubicin.

3.2 Collagenase Conjugation Efficiency and Collagen Degradation

3.2.1 Collagenase Conjugation Efficiency

The incorporation of the components of the nanoparticles was analyzed using FTIR spectra analysis. The C=O stretch can be seen due to carbonyl vibration in the ester linkage in plain PLGA NPs, PLGA-DOX and COL-PLGA-DOX at 1750, 1750 & 1751 cm^{-1}, respectively, indicating the presence of the polymer nanostructure (Figure 3.3 A). The spectrum of DOX shows peaks at 2927 cm^{-1} (C-H bond) and 1076 cm^{-1} (C-O bond). The peaks of DOX are slightly shifted (2965 cm^{-1} and 1083 cm^{-1}) in the PLGA-DOX NPs spectrum and (2960 cm^{-1} and 1083 cm^{-1}) in the COL-PLGA-DOX NP spectrum, respectively, representing the presence of DOX in the PLGA NPs. The characteristic peak for collagenase is seen at 1635 cm^{-1} (Amide I; C=O adsorption), and the peak is also seen at 1640 cm^{-1} on the COL-PLGA-DOX NP spectrum showing collagen conjugation. There is also the presence of Amide-III (C-N stretching) in collagenase at 1235 cm^{-1} and 1265 cm^{-1} in COL-PLGA-DOX NPs. Free collagenase shows an average C-H stretching at 2935 cm^{-1} which is shifted at 2960 cm^{-1} overlapping the C-H stretch due to DOX in COL-PLGA-DOX NPs (Figure 3.3 B).

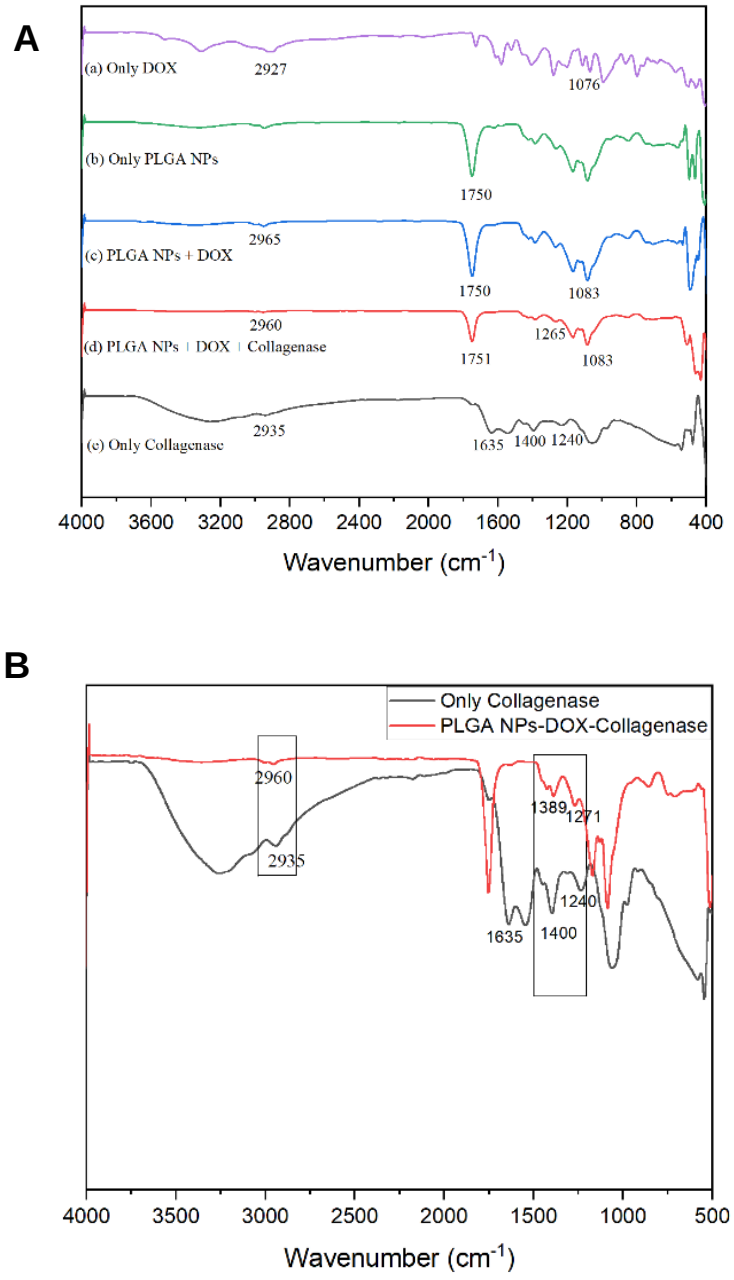

Figure 3.3 FTIR spectra analysis. A) FTIR of free Doxorubicin, plain PLGA NPs, PLGA-DOX NPs, COL-PLGA-DOX NPs, and free collagenase. B) FTIR of free collagenase and COL-PLGA-DOX NPs.

3.2.2 Enzymatic (Collagenase) Degradation of Collagen

Quantitative assessment of collagen degradation by collagenase (1U, 10U, 25U, 100U, 200U, at pH 7.4, after 48 hours) was performed. On average, degrees of degradation (measured by mass loss) rose with the increase of collagenase concentrations (Figure 3.4, Table 3.1), with the highest degradation occurring at ~41% mass loss. One-way ANOVA was performed, and the data was statistically significant between the treatment groups.

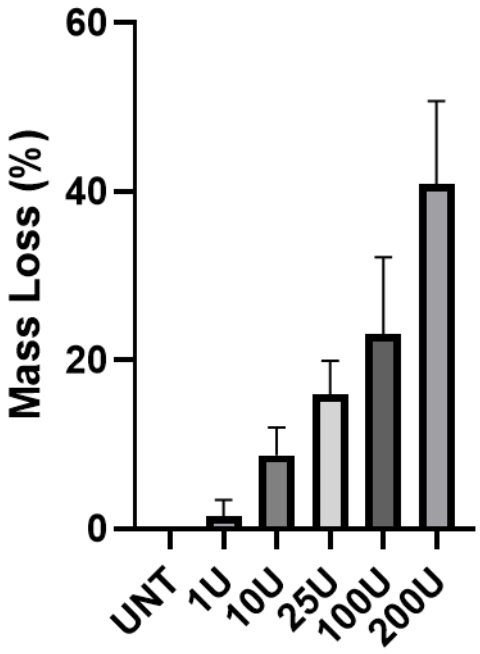

Figure 3.4 Quantitative assessment of collagen degradation by various concentrations of collagenase.

	UNT	1U	10U	25U	100U	200U
% Mass Loss	0	1.5 ± 2.0	8.7 ± 3.3	16 ± 3.9	23 ± 9.1	41 ± 9.9

Table 3.1 Quantitative assessment of collagen degradation by various concentrations of collagenase. Mass loss increases as the concentration of collagenase increases.

3.2.3 COL-PLGA-DOX Degradation of Collagen

Masson's Trichrome staining was used to confirm that decellularized samples were free of cellular contents. Visual inspection of collagen degradation (1, 50, 100, 250, 500, 1000 µg/mL of COL-PLGA-DOX NPs, at pH 7.4 after 48 hours) revealed various levels of collagen degradation across samples, appearing to increase with the rise in concentration (Figure 3.5). Results of the enzymatic collagen degradation data reveals that, at these concentrations of NPs, no significant mass loss would be observed due to the lower conjugation efficiency (58.98%) of collagenase to the surface of the NPs. However, visually and quantitatively, we can observe that collagen degradation is occurring (Figure 3.5, Table 3.2). 1 and 50 µg/mL of COL-PLGA-DOX exhibited the greatest mean area of collagen per field of view, revealing that more collagen is present in these samples. 100, 250, and 500 µg/mL exhibited greater collagen loss, with lesser amounts of

collagen than 1 and 50 µg/mL. There is a large drop in collagen at 1,000 µg/mL, almost half that of the lower doses of COL-PLGA-DOX.

The highest concentration of NPs (1000 µg/mL) carries approximately 0.15U of collagenase. A higher dosage of NP, and therefore, a higher concentration of collagenase, is not clinically feasible because of the high concentration of loaded drug. In the future, the use of collagenase liposomes (collagozomes) could be used in conjunction with COL-PLGA-DOX NPs to target and reduce the fibrotic collagen area [112].

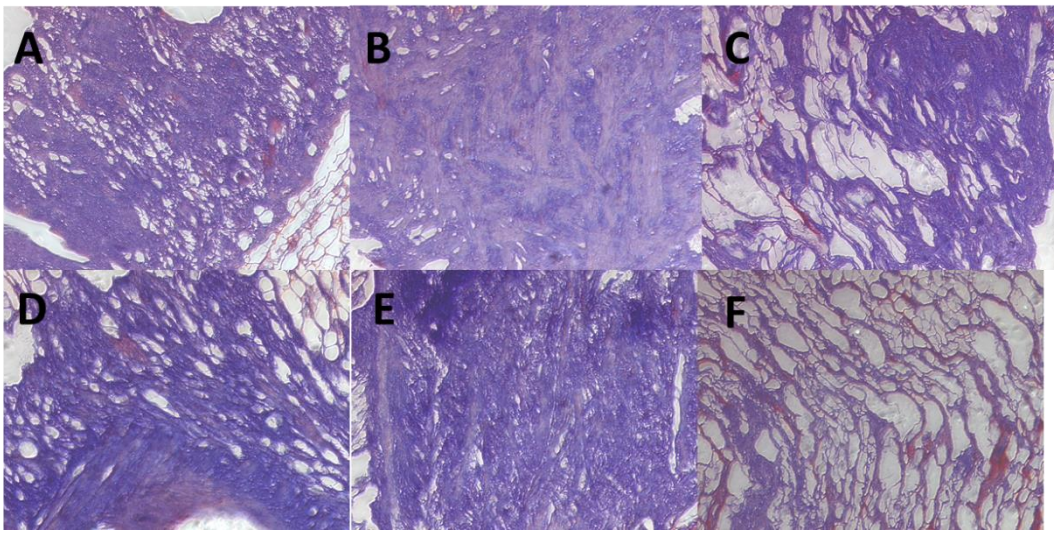

Figure 3.5 Representative images of collagen degradation after treatment with 1 (A), 50 (B), 100 (C), 250 (D), 500 (E), and 1000 (F) µg/mL of COL-PLGA-DOX. Scale bar is 100 µm.

COL-PLGA-DOX Concentration (μg/mL)	Mean Area (μ^2) of Collagen per Field of View
1	3,006,098
50	3,327,066
100	2,265,886
250	2,795,560
500	2,776,416
1,000	1,726,774

Table 3.2 Mean area of collagen per field of view of Masson's Trichrome stained collagen from the decellularized porcine left ventricle following COL-PLGA-DOX treatment.

3.3 *In vitro* Cytocompatibility and Cell Uptake

The cytocompatibility of PLGA NPs at increasing concentrations was determined by MTS assays (Figure 3.6). The PLGA NPs exhibited greater than 70% cytocompatibility at all concentrations with HL1 cardiomyocytes.

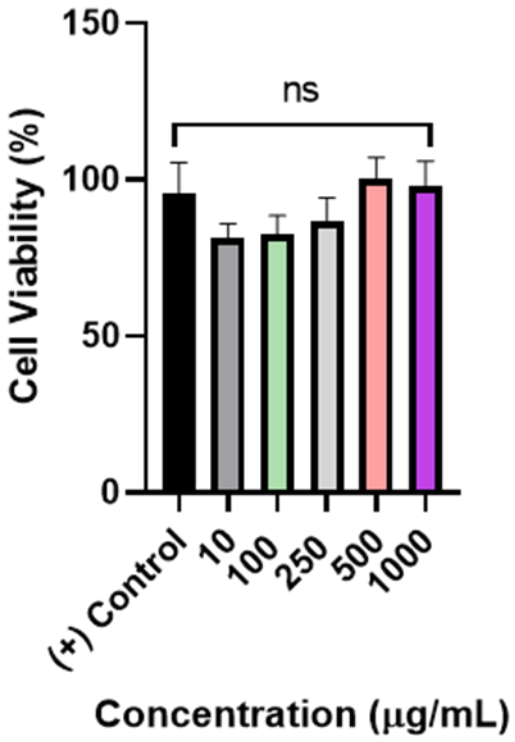

Figure 3.6 Cell viability of PLGA NPs with HL1 cells. Viability increases as NP concentration increases.

HL1 cell uptake of COL-PLGA-DOX NPs was determined by measuring fluorescence (NPs internalized by cells) normalized to the amount of protein (cell number) using a spectrophotometer (Figure 3.7). NPs were taken up by the cell in a dose-dependent manner, with a significantly higher number of NPs taken up at 100 and 250 μg/mL compared to the lower dose of 50 μg/mL. Furthermore, fluorescence microscopy confirmed the dose-dependent response with a much larger accumulation of NPs (green) in HL1 cells with the larger NP doses.

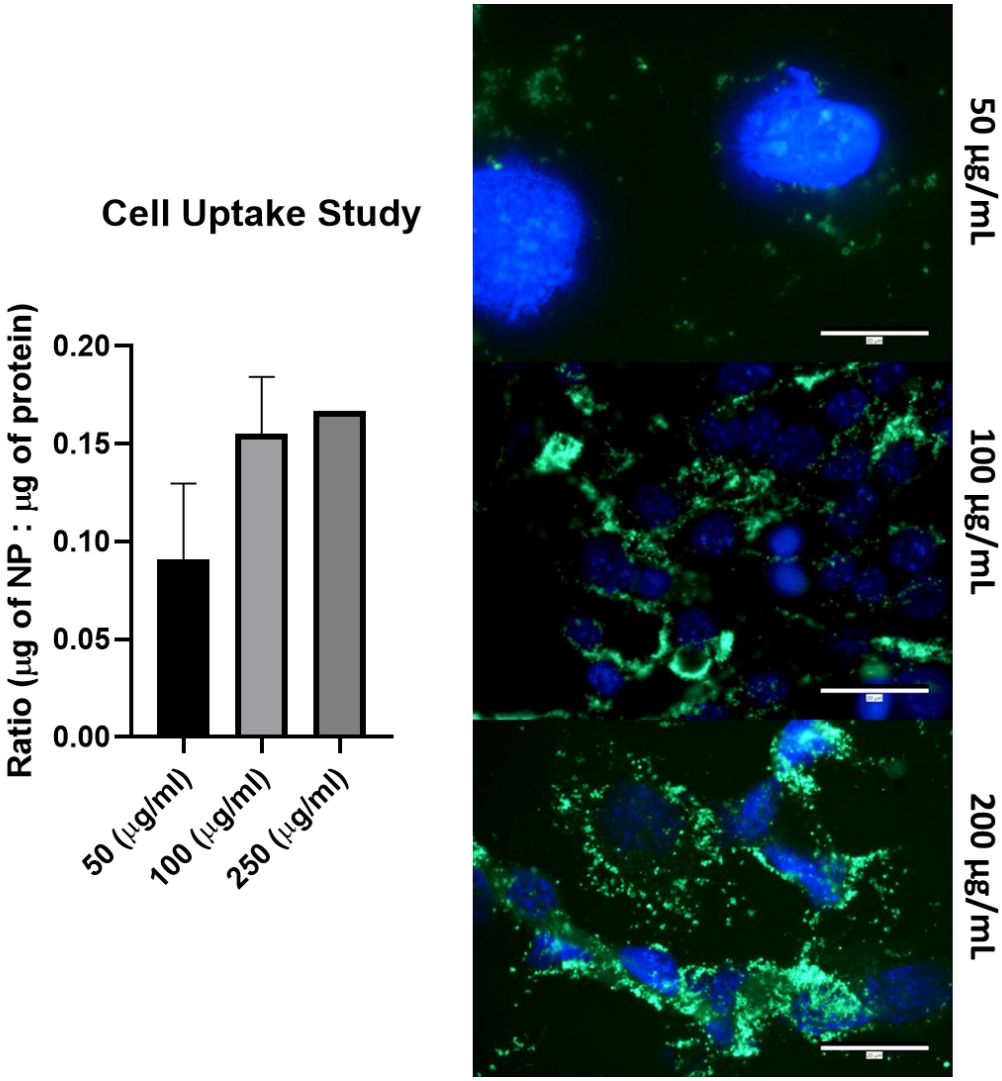

Figure 3.7 Cell uptake study of FITC-labeled NPs. Cell uptake increases as the concentrations of NPs increases.

3.4 *In vitro* Hypertrophic Cell Death

To better determine the therapeutic dose of COL-PLGA-DOX NPs, we performed a picogreen assay to ascertain the IC50 (half maximal inhibitory concentration) of DOX with HL1 cells (Figure 3.8 A). The IC50 of DOX with HL1 cells was found to be 0.4744 μM. Additionally, we determined the IC50 of COL-PLGA-DOX which is used to inhibit exposed heart cells to half their original number (Figure 3.8 B). The IC50 of COL-PLGA-DOX was determined to be 331.8 μg/mL.

The therapeutic efficacy of COL-PLGA-DOX was determined by adding the NPs to the ET-1-stimulated (hypertrophic) HL1 cardiomyocytes and measuring cell death via cytotoxicity assays. Untreated and Triton-X treated cells were used as positive and negative controls, respectively. Cells were treated with free DOX IC50 and IC75 concentrations and NP IC50 (15.3 μg DOX) and IC75 (22.9 μg DOX) concentrations (Figure 3.8 C) for 48 hours. Within 48 hours, COL-PLGA-DOX treatments successfully killed ~80% of cells, like that of free DOX. These results show that our NPs are just as effective as free DOX when added to hypertrophic HL1 cells, although the difference between IC75 and IC50 of COL-PLGA-DOX was not statistically significant. However, altogether, the amount of cell death between all treatment groups compared to the untreated group was statistically significant (p-value = 0.000912).

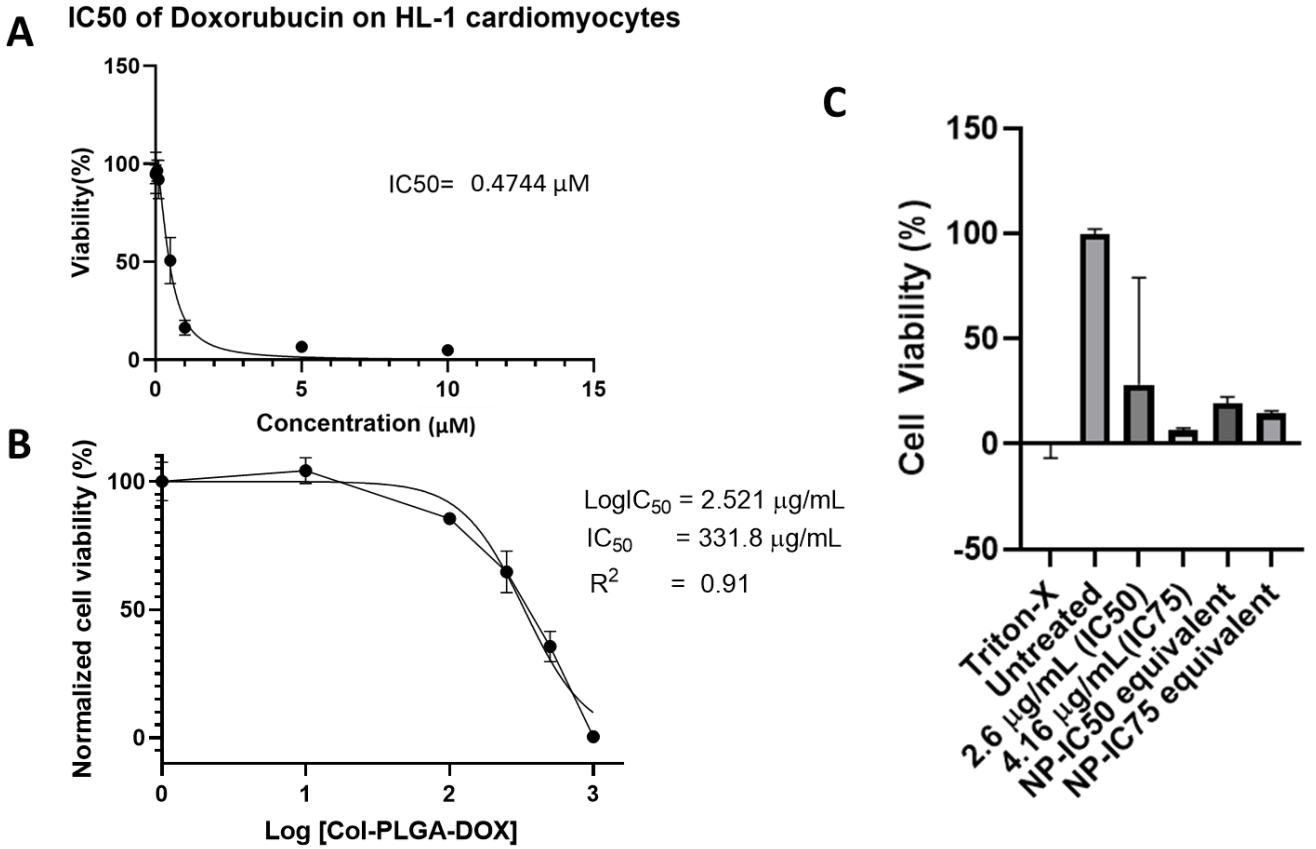

Figure 3.8 A) IC50 of Doxorubicin on HL-1 cardiomyocytes. B) IC50 of COL-PLGA-DOX on HL-1 cardiomyocytes. C) Cell viability after treatment with IC50 and IC75 of free doxorubicin and IC50 and IC75 of COL-PLGA-DOX.

4. Discussion

COL-PLGA-DOX NPs were fabricated using a double emulsion technique and were then fully characterized (Figure 3.2 A, B). The drug release profile showed that within 48 hours, ~50% of the drug was released (Figure 3.2 C). The nanostructure, presence of Doxorubicin, and collagenase conjugation was confirmed by FTIR (Figure 3.3).

Furthermore, collagen degradation studies were performed to determine the efficacy of the nanoparticles to degrade collagen. Using collagenase and increasing NP concentrations, it was determined that at increasing enzymatic units (U, unit for catalytic activity), collagen degradation did occur (Figure 3.4, 3.5 and Table 3.1, 3.2). Quantitative and qualitative assessment of collagen degradation was also observed histologically using Masson's Trichrome stain (blue- collagen, red- heart cells). Note that there were no cells (red) present in the collagen samples to interfere with collagen degradation studies.

Even at the highest concentration of NPs used (1000 µg/mL), there was not enough collagenase to assist in overall collagen mass loss; however, various degrees of degradation are seen histologically, with degradation increasing as the concentration of NPs increases. 1000 µg/mL of NPs is not therapeutically feasible, as it would cause an overabundance

of cell death; therefore, in future studies, the use of collagezomes may be helpful in decreasing the amount of fibrotic collagen *in vivo* [112-114].

Cytocompatibility studies were performed to show that PLGA NPs had no negative effects on the viability of the cells. PLGA NPs had excellent cytocompatibility with HL1 cardiomyocytes (Figure 3.6). Cell uptake of COL-PLGA-DOX NPs showed a dose-dependent response, with more NPs taken up by the cell at higher NP concentrations.

Before beginning *in vitro* studies, the IC50 of DOX (Figure 3.8 A) and IC50 of COL-PLGA-DOX (Figure 3.8 B) with HL1 cardiomyocytes were determined using a picogreen assay. Following this, we performed an *in vitro* HL1 cell death study using the IC50 and IC75 values of COL-PLGA-DOX.

COL-PLGA-DOX NPs were tested in 2D culture on collagen coated plates to determine the effectiveness of the NPs to kill hypertrophied cardiomyocytes in a mimicked collagenous (fibrotic) environment. Within 48 hours of treatment with the IC50 and IC75 of COL-PLGA-DOX (Figure 3.8 C) ~80-85% of cells were killed, similar to the rate of death caused by free, untargeted Doxorubicin, showing the success of these NPs in killing hypertrophied cells in a collagenous environment.

The *in vitro* results of these studies showed that our NP system can successfully kill hypertrophied cells; however, future studies should be performed *in vivo* to visualize the results in a living organism.

5. Future Studies and Conclusions

Future studies should be carried out to test the enzyme activity of collagenase following conjugation to the NPs. Some loss of enzyme activity is expected. If collagenase does not prove to be a successful targeting tool *in vivo*, studies should be performed using qPCR to determine overexpression of mRNAs and resulting proteins that could be used for targeting.

Additionally, brain natriuretic peptide (BNP) can be used to study the hypertrophic cardiomyocytes and any resulting damage. BNPs are produced by the heart, and higher levels of BNPs have been associated with cardiac hypertrophy [115]. BNPs may be used as a marker for cardiac hypertrophy and any resulting tissue remodeling.

Furthermore, cell death by Doxorubicin has been carried out by either apoptosis or necrosis [116]. It is important to study which mechanism of cell death is used *in vivo*, which could determine efficacy of our NP

ablation system. As the first FDA-approved nano-drug, Doxorubicin-loaded NPs hold much promise in our ablation system. Ammonium sulfate has been used to in conjunction with Doxorubicin to increase and retain Doxorubicin in liposomes. When combined with ammonium sulfate, the drug mixture crystallizes and aggregates forming a more stable structure [117].

To verify hypertrophied cell death, fibrotic collagen remodeling and/or dissolution, and nanoparticle localization following treatment with COL-PLGA-DOX, an *in vivo* study should be performed using an HCM mouse model. DBA/2J mouse models have been used for HCM modeling because of the mutations found in MyBPC-3 and MyH7, two hallmarks of HCM. Following a thoracotomy, NPs will be injected directly into the hypertrophied septum using a syringe and needle. Echocardiography can serve as a means to measure cardiac function at different time points, before and after NP treatment. After euthanasia, mouse hearts should be examined to assess cell death, collagen degradation, and nanoparticle localization using immunohistochemistry and histology. For the biodistribution study, COL-PLGA-Cy5 and plain PLGA-Cy5 (control) particles could be used to determine the localization ability of collagenase-coated particles.

In conclusion, we have developed a COL-PLGA-DOX NP drug delivery system to replace the ASA procedure with a more effective therapeutic option for HCM. The ET-1 stimulated HL1 cardiomyocytes were treated with COL-PLGA-DOX for 48 hours in culture medium and were able to release ~50% of the loaded drug as determined by the drug release profile. Additionally, PLGA NPs showed excellent cytocompatibility with HL1 cells, as well as a concentration-dependent uptake into hypertrophic HL1 cardiomyocytes. The COL-PLGA-DOX drug delivery system possibly in conjunction with collagezomes, if given the opportunity, has the ability to enhance the therapeutic efficacy for HCM treatment.

CHAPTER 4

Regulation of the Spatial Distribution of Hypertrophic Cardiomyopathy Treatments Using Nanoparticles

Abstract

Introduction. Alcohol septal ablation, as a treatment option for hypertrophic cardiomyopathy, is often used for the particularly vulnerable HCM patient population. However, it has many downfalls, especially excessive healthy myocardial cell death. To fight this clinical challenge, we have designed a targeted nanoparticle delivery system that is localized to the diseased septum. To determine if these nanoparticles are indeed localized, we have performed an *ex vivo* study with a pig heart model to compare the spatial distribution of alcohol, untargeted nanoparticles, and targeted nanoparticles.

Methods and Results. Cy5 PLGA nanoparticles and collagenase coated Cy5 PLGA nanoparticles were prepared using a standard double emulsion technique. An alcohol-Cy5 mixture was used as a control. All groups were delivered directly to the septum using a 21-gauge needle. We found that alcohol covered much more regions than the nanoparticles, diffusing downward and outward from the injection site. Both nanoparticle groups appeared to be localized to the area surrounding the injection site.

Conclusion. Our targeted nanoparticle treatment system has shown to have better localization capability than alcohol and untargeted NPs. These results may influence the future of patient healthcare for patients with HCM.

1. Introduction

Hypertrophic Cardiomyopathy (HCM) is a potentially fatal disease that can affect as many as 1/200 people [7, 8, 118-120]. Patients with HCM experience thickened septums, larger than 13 mm, which disrupts the left ventricular outflow tract, leading to obstruction. These issues may affect cardiac function resulting in serious problems such as arrythmias and/or heart failure [1, 3, 7, 11, 87, 121]. As a result of the extra stress placed on the heart, collagenous fibrosis is a major concern. Cardiothoracic surgeons often recommend removal of the overgrown septum by septal myectomy, which is the gold standard treatment option. For the especially vulnerable HCM patient population, alcohol septal ablation (ASA) is often recommended [41, 122-124]. ASA is an outpatient procedure in which cardiologists deliver absolute alcohol directly to the diseased septum through a catheter. When given the option between surgery and ASA, most patients prefer ASA because it has lower periprocedural risks than surgery [38]. Although ASA is the treatment of choice to most well-informed patients, it has many downfalls including healthy myocardial cell death due to lack of localization of alcohol. To combat these localization issues, we have developed a nanoparticle (NP) system that targets the fibrotic extracellular

matrix (collagen) of the diseased tissue after local delivery. To determine the localization patterns of our targeted NPs, we performed an *ex vivo* study using a pig model to measure the mean area that each group covers on the anterior and posterior aspects of the cardiac septum. Using ImageJ thresholding analysis, we were able to determine the localization capability of each group. This important data may be influential for the future treatment of HCM.

2. Experimental Section

2.1 Materials

Porcine hearts were purchased from a local abattoir (Fischer's Meat Market, Muenster, TX) and were immediately transported to the University of Texas at Arlington in PBS and on ice. The hearts were promptly dissected to uncover the uppermost septal perforator along the left anterior descending coronary artery. Cy5 was purchased from Lumiprobe (Hunt Valley, Maryland USA).

2.2 Fabrication of PLGA-Cy5 Nanoparticles

Cy5 NPs were prepared by a standard double emulsion process. Briefly, 100 mg of PLGA (90% PLGA 50:50, 10% PLGA-NHS) was dissolved in 3 mL DCM. PLGA-NHS was used to allow for conjugation of COL to the surface of the NPs which will be described later. Cy5 was dissolved in dimethyl sulfoxide (DMSO) and was added dropwise to the PLGA solution on a stir plate at room temperature. The resulting emulsion was sonicated on ice for 3 minutes at 30 watts and was then added to 5% PVA on a stir plate overnight at room temperature. The solution was then ultrasonicated at 25 amps. After overnight stirring, the NPs were washed with deionized water and were collected by centrifugation and lyophilization.

To conjugate collagenase (COL) to the surface of the Cy5 particles, 20 µg (per 10 mg of NPs) of COL were added to a NP solution in PBS (1 mg/mL). The solution was incubated overnight at 4°C. Following the incubation, the NPs were collected by ultracentrifugation at 15,000 rpm for 30 minutes. The supernatant was used to determine peptide conjugation efficiency. Pellets were resuspended in DI water and were lyophilized resulting in the final COL-PLGA-Cy5 NPs.

2.3 Characterization of Nanoparticles

Using a dynamic light scattering (DLS) technique, particle size and surface charges were measured using a ZetaPALS zeta potential analyzer (Brookhaven Instruments Inc.). The morphology of the particles was also analyzed using transmission electron microscopy (TEM, JOEL 1200EX). A drop of particle solution (2 mg/mL) was placed on a Formvar-coated 200-mesh copper grid (Electron Microscopy Sciences,Hartfield, PA) at room temperature and allowed to air-dry followed by treatment with 0.1% uranyl acetate solution. The sample was then inserted into the TEM instrument for observation.

2.4 Collagenase Conjugation Efficiency

Collagenase conjugation was confirmed by Fourier-transform infrared spectroscopy (FTIR) which was previously reported in Chapter 3.

2.5 *Ex vivo* Delivery of Nanoparticles

1 mL of each COL-Cy5 and Cy5 NP solutions were injected into the septum via the uppermost septal perforator of the left anterior descending coronary artery using a 21-gauge needle. After delivery, images were taken

of the hearts using a custom-built fluorescent microscope. 1 mL of Cy5-Ethanol hearts were used as a control. After the initial image, each heart was washed with PBS and reimaged to capture how the NPs could migrate under fluid flow. After PBS washing, the scope of the ablation solution reaching can be estimated by the Cy5 signals shown on the fluorescent image of the heart. Quantitatively, we used the area of Cy5 signal on images of each group to assess whether the solution was diffusing from the injection site or staying close the injection site (localized delivery). The Cy5 signal area were calculated by thresholding the fluorescent images using ImageJ (Rasband, W.S., ImageJ, U. S. National Institutes of Health, Bethesda, Maryland, USA, https://imagej.nih.gov/ij/, 1997-2018.).

2.6 Statistical Analyses

All values are reported as the mean ± standard deviation (SD), where a p-value less than 0.05 was considered as statistically significant. One-way analysis of variances (ANOVA) was performed to quantify the statistical significance of COL-Cy5 delivery, Cy5 NP delivery, and alcohol delivery. All statistical analyses were conducted in RStudio (R Foundation for Statistical Computing, Vienna, Austria).

3. Results

3.1 Nanoparticle Characteristics

The biodegradable PLGA nanoparticles were fabricated using a double emulsion technique. The PLGA-Cy5 and COL-PLGA-Cy5 NPs had a mean diameter of 204 ± 37.7 nm and 280 ± 45.2 nm, respectively (Figure 4.1 A). The zeta potentials of PLGA-Cy5 and COL-PLGA-Cy5 were -9.4 ± 3.7 mV and -25 ± 3.7 mV, respectively. TEM images revealed a spherical, smooth morphology for both NP groups (Figure 4.1 B,C).

A

	Size (nm)	Charge (mV)
PLGA-Cy5	204 ± 37.7	-9.4 ± 3.7
COL-PLGA-Cy5	280 ± 45.2	-25 ± 3.7

B

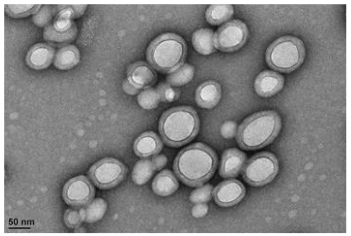

C

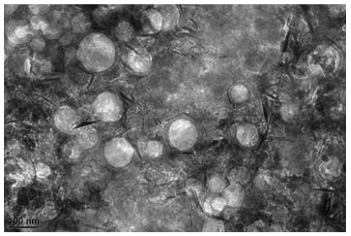

Figure 4.1 A) Size and charge of PLGA-Cy5 and COL-PLGA-Cy5 NPs. B) Representative TEM image of PLGA-Cy5 NPs. C) Representative TEM image of COL-PLGA-Cy5 NPs.

3.2 Collagenase Conjugation Efficiency

Collagenase conjugation efficiency was confirmed by FTIR as previously reported in Chapter 3. The conjugation efficiency was approximately 60%.

3.3 *Ex vivo* Delivery and Spatial Distribution of Nanoparticles

1 mL of Cy5-Alcohol, PLGA-Cy5, or COL-PLGA-Cy5 was delivered via the uppermost septal perforator (Figure 4.2 A, orange arrow) with a 21-gauge needle. The purpose of this experiment was to determine the localization ability of COL-PLGA-Cy5 compared to absolute alcohol, which is used in alcohol septal ablation. As previously mentioned, alcohol is not specifically localized to the septal tissue which results in alcohol expanding into healthy tissues. Our results indicate that, when delivered via a septal perforator, alcohol covers an anterior and posterior septal surface area of 390 ± 10 cm^2 (Figure 4.2 B,C). PLGA-Cy5, on the other hand, covered 94 cm^2 (Figure 4.2 D,E) while COL-PLGA-Cy5 covered the least amount of area, 61 ± 8.5 cm^2 (Figure 4.2 F,G). PLGA-Cy5 and COL-PLGA-Cy5 appeared to localize close to the injection site, while alcohol dispersed downwards and outwards.

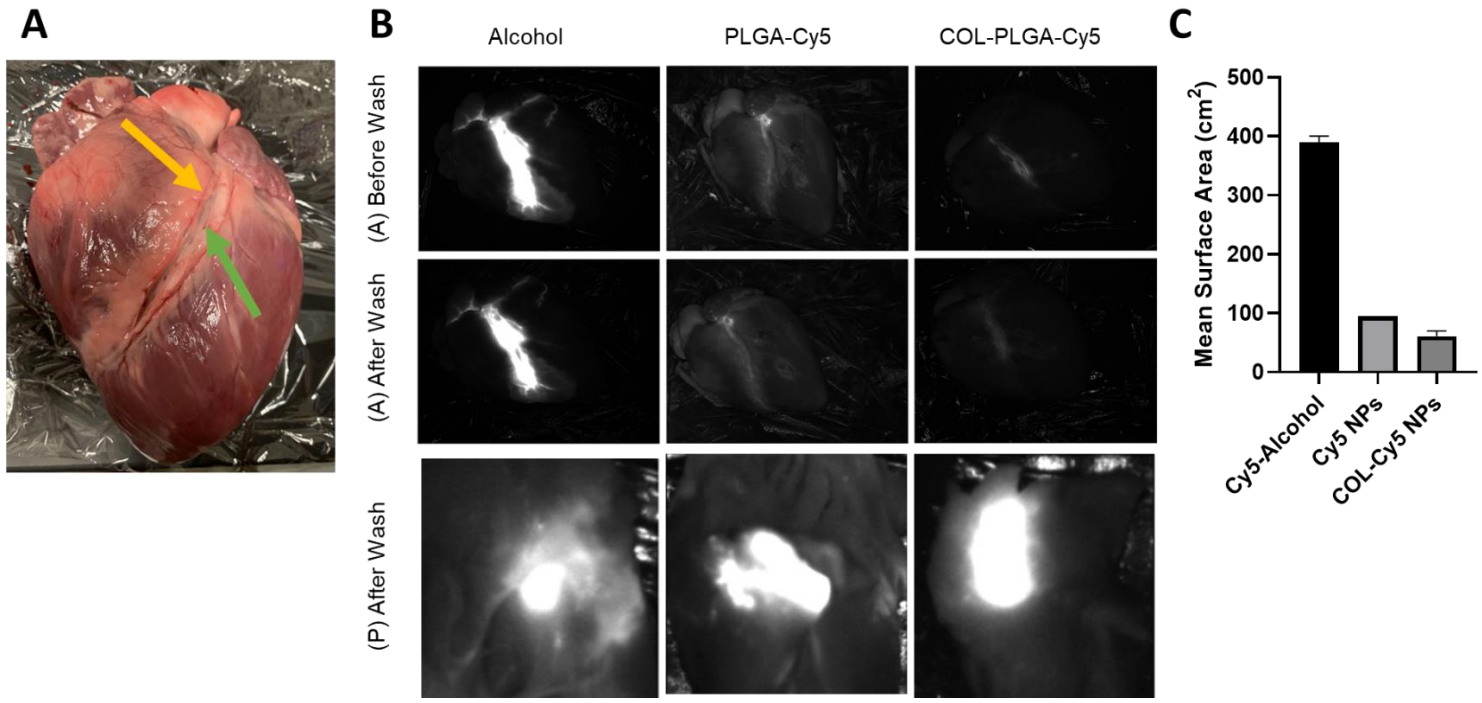

Figure 4.2 A) Injection site of treatment groups (orange arrow) and visible septal perforator (green arrow). B) Anterior (A) and Posterior (P) view following treatment with Cy5-Alcohol. C) Mean surface area covered of alcohol, PLGA-Cy5, and COL-PLGA-Cy5 after treatment to the septum.

4. Discussion

PLGA-Cy5 and collagenase coated PLGA-Cy5 (COL-PLGA-Cy5) NPs were fabricated using a double emulsion technique. PLGA-Cy5 NPs had an average diameter of 204 ± 37.7 nm and an average charge of -9.4 ± 3.7 mV (Figure 4.1 A). COL-PLGA-Cy5 NPs had an average size of 280 ± 45.2 nm with an average charge of -25 ± 3.7 mV (Figure 4.1 A). An alcohol-Cy5 mixture was used as a control and the NPs served as our treatment groups. After delivery of control and treatment groups to the cardiac septum via a 21-gauge needle (Figure 4.2 A), a PBS wash was administered. Following the PBS wash, mean surface area was calculated using thresholding in ImageJ. Overall, alcohol proved to cover much more surface area than the NPs (Figure 4.2 B), with a significant difference (one-way ANOVA, $p = 0.001495$). COL-PLGA-Cy5 NPs covered the least amount of surface area, not straying far from the injection site. When compared to the delivery of pure alcohol, our untargeted and targeted NP system appears to remain close to the injection site, while alcohol diffuses outwards and downwards. This may mean, in the future, that multiple NP injections through septal perforators may be needed to cover the full diseased septal area. This also gives cardiologists the freedom to inject the NPs only at the infected areas without risk of the NP traveling into healthy tissues. Another point to consider is the size of the NPs. COL-PLGA-Cy5

NPs were larger than PLGA-Cy5 particles, which may have decreased the diffusion effects making them cover less surface area. For HCM localized treatment, larger NPs may be favorable over smaller NPs.

5. Conclusion

Our targeted NP treatment system has shown to have better localization capability than the treatments with alcohol and untargeted NPs, covering the least amount of area. For this study, we used healthy porcine hearts, which is a limitation; however, as a proof-of-concept study the reported results demonstrated a localized spatial distribution of NPs and formed a strong foundation for future validation using diseased tissues or *in vivo* model. The results of this study may influence the future of patient healthcare for patients with HCM.

CHAPTER 5

CONCLUSIONS AND FUTURE WORK

5.1 Conclusions

5.1.1 Ultrastructural and Mechanical Characterization of Human Healthy and Hypertrophic Cardiac Septal Tissues

As seen by our ultrastructural and mechanical observations, the overexpressed, disorganized fibrotic ECM present in HCM tissues has a direct influence on the overall mechanical properties. By ultrastructural analysis using Masson's Trichrome staining, we were able to quantify cell size and cell and collagen fiber disarray. Cell size was much larger in HCM hearts than their healthy counterparts, and disarraying of cells and disorganized over-expressed fibrotic collagen fibers were important structural alterations in HCM. We further demonstrated that the healthy septal tissues had a nonlinear, anisotropic, and viscoelastic mechanical behavior, in which the collagen network was well organized at ultrastructural level and well-integrated with heart muscle cells. As a result, the healthy septal tissues had an optimal nonlinear concave upward stress-strain curve, in which the tissue could be easily extended at lower stress level, while at

higher stress level the gradually-recruited collagen fiber network eventually served as a locking-up mechanism to protect the muscle fibers from debonding and tear. The poorly organized, pathological fibrotic compositions in HCM disrupted the optimal native tissue design and resulted in an inferior mechanical behavior, in which the over-expressed, disorganized collagen fibers increased the initial tensile modulus, shear modulus, energy dissipation, while greatly decreasing tissue mechanical strength and diminishing the J shape nonlinearity of stress-strain curve, i.e., a cell protection mechanism.

5.1.2 Nanoparticle-Mediated Controlled Myocardial Drug Delivery

We have developed a COL-PLGA-DOX NP system, with a goal to replace the ASA procedure. Hypertrophic cardiomyocytes were treated with COL-PLGA-DOX for 48 hours in 2D culture on collagen coated plates (Figure 3.1, Figure 3.8 C). Over a period of 48 hours, NPs were able to kill ~80-85% of hypertrophied cells (Figure 3.8 C). It is assumed that more than 50% of DOX was released as determined by the drug release profile (Figure 3.1 C). The PLGA component of the NPs were not responsible for cell death, seen by the cytocompatibility study with HL1 cells (Figure 3.6). Additionally, the NPs showed a concentration-dependent uptake of NPs by

the cardiomyocytes (Figure 3.7). As the concentration of NPs increased, uptake by the cells also increased. Quantitative and qualitative assessment of collagen degradation showed an increase in collagen degradation as the concentration of collagenase increased (Figures 3.4, 3.5, Table 3.1). However, although COL may serve well as a targeting agent, the amount of COL (collagenase) carried by NPs may not be sufficient to decrease the large mass of the collagen found in the HCM septum. In cases where the presence of abundant collagen is a problem, the use of collagezomes may be useful in decreasing the amount of collagen present in the HCM cardiac septal tissue. The COL-PLGA-DOX drug delivery system in conjunction with collagezomes, if given the opportunity, has the ability to enhance the therapeutic efficacy for HCM treatment.

5.1.3 Regulation of the Spatial Distribution of Hypertrophic Cardiomyopathy Treatments Using Nanoparticles

Pure alcohol, PLGA-Cy5, and COL-PLGA-Cy5 NPs were delivered to the porcine septum using a 21-gauge needle (Figure 4.2 A) in a manner like the ASA procedure. Our targeted NP system remained localized to the injection site, while the alcohol-Cy5 mixture diffused outwards and downwards from the injection site (Figure 4.2 B). Although we used healthy

porcine hearts for this study, the results are still indicative of how NPs will react when injected into the cardiac septum, thereby, influencing the future of treatment of HCM for the vulnerable population, and for those who choose the septal ablation technique over surgery.

5.2 Future Work

In relation to our NP system, studies should be carried out to determine if collagenase is the best targeting system for our NP ablation system. qPCR should be used to determine mRNAs and any resulting proteins that may be overexpressed and can be used for cell-targeting therapies. Furthermore, higher levels of brain natriuretic peptides (BNPs) may be used as a biomarker for cell hypertrophy and can aid us in studying hypertrophied cardiomyocytes, and as a biomarker to monitor the degree of targeted ablation of the hypertrophied cardiomyocytes. Furthermore, Doxorubicin has been shown to induce cell death by either apoptosis and/or necrosis. The mechanism of cell death by Doxorubicin should be studied using *in vivo* animal models as other *in vivo* factors may disrupt the efficacy of our NP ablation system.

In vivo studies should focus on the assessment of the safety and effectiveness of the newly developed ablation NPs using an HCM mouse

model. DBA/2J (D2) strain of mice can be used as the *in vivo* HCM model due to their sequence variants in *MYBPC3* and *MYH7*, two key features of human HCM [125]. A sham surgery should be used as the baseline control for the treatment groups. A thoracotomy need to be performed on all groups. Treatments can be delivered directly to the septum via a syringe and needle. Following injection, the chest will be closed in successive layers and enough time should pass for the mice to recover.

All experimental procedures related to performance can be undertaken through cardiac ultrasound using a high-resolution ultrasound imaging system. Anesthesia should be induced with 3.0% isoflurane and maintained with 1.5% isoflurane. Experimental animals should be secured, and body temperature maintained at 36-38°C. Heart rate can be monitored via a transcutaneous electrode. Images obtained in left- and right-parasternal long- and short-axis views will be measured to calculate ejection fraction (EF) and fractional shortening (FS). LV linear dimensions in systole and diastole are measured from short-axis views and used to calculate FS. Left ventricular volumes and ejection fraction (EF) are calculated from direct measurement of left ventricular area in systole and diastole using a modified apical 2- chamber view. LVEF is expressed as: $EF = \frac{LVVd^2 - LVVs^2}{LVVd^2 \times 100}$ (%). The left ventricular systolic shortening fraction (LVFS) is expressed as: $FS =$

$\frac{LVDd-LVDs}{LVDd\times 100}$ (%). Population data should be analyzed using an analysis of variance (ANOVA) test followed by Bonferroni's correction. Tests with p-values less than 0.05 will be judged as significant.

All animal experiment protocols should be approved by Animal Care and Usage Committee. An HCM mouse model will be used to determine the biodistribution of COL-PLGA-Cy5, as well as the specificity of these NPs to collagen of the heart. Following NP and control group (ethanol or untargeted NPs) injection, the whole body should be captured at different time points using an *in vivo* imaging system. NP and control group biodistribution should be performed and histological analysis should be carried out. Biodistribution can be evaluated using immunofluorescence, immunohistochemical, and histological staining techniques to evaluate the localization of the NPs in the diseased area (hearts) and to observe the method of NP clearance from the body (livers, kidneys, and blood samples). Additionally, NP-treated and control hearts should be weighed in comparison to the untreated hearts from similar-sized mice to determine heart mass loss. Cell death and collagen degradation can be examined through histology. Histological sections will allow us to assess the amount of cell death and the range of cell death. To do this, 5-10 µm thick cryosections will be made and microscopic images will be taken utilizing a

fluorescence microscope combined with a CCD camera. Immunofluorescence and histological staining will reveal the level of cell death and collagen degradation in treatment groups as compared to the control groups. Additionally, the method of heart cell death will be revealed by immunohistochemistry (apoptotic or necrotic).

The proposed *in vivo* study will eventually enable the direct testing of our hypothesis, which is that the delivery of our novel Doxorubicin-loaded, collagenase-coated, (COL-PLGA-DOX) degradable nanoparticles will enable a breakdown of the fibrotic network in HCM tissue and allow an efficient localized Doxorubicin-induced killing of the hypertrophic cardiomyocytes, and hence shrink the overgrown HCM septal tissue.

REFERENCES

1. A.J.Marian, R.R., *The Molecular Genetic Basis for Hypertrophic Cardiomyopathy* J Mol Cell Cardiol, 2001. **33**: p. 655-670.
2. Kimura, A., et al., *Mutations in the cardiac troponin I gene associated with hypertrophic cardiomyopathy.* Nature genetics, 1997. **16**(4): p. 379-382.
3. Semsarian, C., et al., *New perspectives on the prevalence of hypertrophic cardiomyopathy.* Journal of the American College of Cardiology, 2015. **65**(12): p. 1249-1254.
4. Kraft, T., et al., *Familial hypertrophic cardiomyopathy: functional effects of myosin mutation R723G in cardiomyocytes.* Journal of molecular and cellular cardiology, 2013. **57**: p. 13-22.
5. Maron, B.J., M.S. Maron, and C. Semsarian, *Genetics of hypertrophic cardiomyopathy after 20 years: clinical perspectives.* Journal of the American College of Cardiology, 2012. **60**(8): p. 705-715.
6. Staff, M.C. *Hypertrophic Cardiomyopathy*. 2020 6/2/2020 [cited 2020 8/19/2020]; Available from: https://www.mayoclinic.org/diseases-conditions/hypertrophic-cardiomyopathy/symptoms-causes/syc-20350198.

7. Marian, A.J. and E. Braunwald, *Hypertrophic cardiomyopathy: genetics, pathogenesis, clinical manifestations, diagnosis, and therapy.* Circulation research, 2017. **121**(7): p. 749-770.

8. Perry M. Elliott, M., Jan Poloniecki, DPHIL, Shaughan Dickie, Sanjay Sharma, BSC, MRCP, Lorenzo Monserrat, MD, Amanda Varnava, MRCP, Niall G. Mahon, MD, MRCPI, William J. McKenna, MD, FRCP, FACC, FESC, *Sudden Death in Hypertrophic Cardiomyopathy: Identification of High Risk Patients.* J Am Coll Cardiol, 2000. **36**(7): p. 2212-2218.

9. Bagnall, R.D., et al., *Whole Genome Sequencing Improves Outcomes of Genetic Testing in Patients With Hypertrophic Cardiomyopathy.* J Am Coll Cardiol, 2018. **72**(4): p. 419-429.

10. Okutucu, S., K. Aytemir, and A. Oto, *Glue septal ablation: A promising alternative to alcohol septal ablation.* JRSM cardiovascular disease, 2016. **5**: p. 2048004016636313.

11. Helms, A.S., et al., *Sarcomere mutation-specific expression patterns in human hypertrophic cardiomyopathy.* Circulation: Cardiovascular Genetics, 2014. **7**(4): p. 434-443.

12. Semsarian C, I.J., Maron MS, Maron BJ, *New perspectives on the prevalence of hypertrophic cardiomyopathy.* J Am Coll Cardiol, 2015. **65**(12): p. 1249-1254.

13. Maron, B.J., *Hypertrophic Cardiomyopathy: A Systematic Review.* The Journal of the American Medical Association, 2002. **287**(10): p. 1308-1320.

14. O'Mahony, C., et al., *A novel clinical risk prediction model for sudden cardiac death in hypertrophic cardiomyopathy (HCM risk-SCD).* Eur Heart J, 2014. **35**(30): p. 2010-20.

15. Guttmann, O.P., et al., *Atrial fibrillation and thromboembolism in patients with hypertrophic cardiomyopathy: systematic review.* Heart, 2014. **100**(6): p. 465-72.

16. O'Hanlon R, G.A., Roughton M, Moon JC, Clark S, Wage R, Webb J, Kulkarni M, Dawson D, Sulaibeekh L, Chandrasekaran B, Bucciarelli-Ducci C, Pasquale F, Cowie MR, McKenna WJ, Sheppard MN, Elliott PM, Pennell DJ, Prasad SK., *Prognostic significance of myocardial fibrosis in hypertrophic cardiomyopathy.* J Am Coll Cardiol, 2010. **56**(11): p. 867-874.

17. Maron, B.J., et al., *Hypertrophic cardiomyopathy.* New England Journal of Medicine, 1987. **316**(14): p. 844-852.

18. Firoozi, S., et al., *Septal myotomy-myectomy and transcoronary septal alcohol ablation in hypertrophic obstructive cardiomyopathy. A comparison of clinical, haemodynamic and exercise outcomes.* Eur Heart J, 2002. **23**(20): p. 1617-24.

19. Marian, A.J., *Hypertrophic cardiomyopathy: from genetics to treatment.* Eur J Clin Invest, 2010. **40**(4): p. 360-9.

20. Charles L. Mclntosh, M., PhD, and Barry J. Maron, MD, *Current Operative Treatment of Obstructive Hypertrophic Cardiomyopathy.* Clinical Progress Series, 1988. **78**(3): p. 487-495.

21. Paolo Spirito, M.D., Christine E. Seidman, M.D., William J. McKenna, M.D., and Barry J. Maron, M.D., *The Management of Hypertrophic Cardiomyopathy.* N Engl J Med 1997. **336**: p. 775-785.

22. E. Douglas Wigle, H.R., Brian P. Kimball, and William G. Williams, *Hypertrophic Cardiomyopathy Clinical Spectrum and Treatment.* American Heart Association, 1995. **92**(7): p. 1680-1692.

23. Ostman-Smith, I., et al., *Age- and gender-specific mortality rates in childhood hypertrophic cardiomyopathy.* Eur Heart J, 2008. **29**(9): p. 1160-7.

24. J. Kosutic, D.Z., *High-Dose Beta-Blocker Hypertrophic Cardiomyopathy Therapy in a Patient with Friedreich Ataxia.* Pediatric Cardiology, 2005. **226**: p. 227-230.

25. Rosso, R., et al., *Calcium channel blockers and beta-blockers versus beta-blockers alone for preventing exercise-induced*

arrhythmias in catecholaminergic polymorphic ventricular tachycardia. Heart Rhythm, 2007. **4**(9): p. 1149-54.

26. Douglas R. Rosing, M., Ulla Idänpään-Heikkilä, MD, Barry J. Maron, MD, Robert O. Bonow, MD, Stephen E. Epstein, MD, *Use of calcium-channel blocking drugs in hypertrophic cardiomyopathy.* The American Journal of Cardiology, 1985. **55**(3): p. 185-195.
27. Serfas D, S.D., Lorell BH, *Phaeochromocytoma and hypertrophic cardiomyopathy: apparent suppression of symptoms and noradrenaline secretion by calcium-channel blockade.* Lancet, 1983. **24**(2): p. 711-713.
28. Douglas R. Rosing, M.D., Kenneth M. Kent, M.D., PH.D., Jeffrey S. Borer, M.D., and M.D. Stuart F. Seides, Barry J. Maron, M.D., Stephen E. Epstein, M.D., *Verapamil Therapy: A New Approach to the Pharmacologic Treatment of Hypertrophic Cardiomyopathy I. Hemodynamic Effects.* American Heart Association, 1979. **60**(6): p. 1201-1207.
29. Coppini, R., et al., *Late sodium current inhibition reverses electromechanical dysfunction in human hypertrophic cardiomyopathy.* Circulation, 2013. **127**(5): p. 575-84.
30. GM, V., *Role of DNA testing for diagnosis, management, and genetic screening in long QT syndrome, hypertrophic*

cardiomyopathy, and Marfan syndrome. Heart, 2001. **86**(1): p. 12-14.

31. Paul Dorian, M., *Antiarrhythmic Action of β-Blockers: Potential Mechanisms.* J Cardiovasc Pharmacol Therapeut, 2005. **10**: p. 15-22.
32. Smedira, N.G., et al., *Current effectiveness and risks of isolated septal myectomy for hypertrophic obstructive cardiomyopathy.* Ann Thorac Surg, 2008. **85**(1): p. 127-33.
33. Ommen, S.R., et al., *Long-term effects of surgical septal myectomy on survival in patients with obstructive hypertrophic cardiomyopathy.* J Am Coll Cardiol, 2005. **46**(3): p. 470-6.
34. Maron, B.J., et al., *Why we need more septal myectomy surgeons: An emerging recognition.* J Thorac Cardiovasc Surg, 2017. **154**(5): p. 1681-1685.
35. Group, M.R. *Global Cardiac Catheters Market 2017 - Production, Sales, Supply, Demand, Analysis & Forecast to 2021*. 2018 [cited 2018; Available from: http://www.mrsresearchgroup.com/market-analysis/global-cardiac-catheters-market-2017-production-sales-supply.html.

36. Spirito, P., J. Rossi, and B.J. Maron, *Alcohol septal ablation: in which patients and why?* Ann Cardiothorac Surg, 2017. **6**(4): p. 369-375.

37. Sherif F. Nagueh, M., Bertron M. Groves, MD, Leonard Schwartz, MD, Karen M. Smith, MD,, et al., *Alcohol Septal Ablation for the Treatment of Hypertrophic Obstructive Cardiomyopathy.* Journal of the American College of Cardiology, 2011. **58**(22).

38. Fifer, M., *Most fully informed patients choose septal ablation over septal myectomy [Controversies in Cardiovascular Medicine].* Circulation, 2007. **116**: p. 207-216.

39. Alam M, D.H., Lakkis N, *Alcohol septal ablation for hypertrophic obstructive cardiomyopathy: a systematic review of published studies.* J Interv Cardiol, 2006. **19**(4).

40. Talreja DR, N.R., Edwards WD, Valeti US, Ommen SR, Tajik AJ, Dearani JA, Schaff HV, Holmes DR Jr., *Alcohol septal ablation versus surgical septal myectomy: comparison of effects on atrioventricular conduction tissue.* J Am Coll Cardiol., 2004. **44**(12).

41. Holmes DR Jr, V.U., Nishimura RA, *Alcohol septal ablation for hypertrophic cardiomyopathy: indications and technique.* Format: AbstractSend to Catheter Cardiovasc Interv. , 2005. **66**(3).

42. Veselka, J., et al., *Complications of low-dose, echo-guided alcohol septal ablation.* Catheter Cardiovasc Interv, 2010. **75**(4): p. 546-50.

43. ten Cate, F.J., et al., *Long-term outcome of alcohol septal ablation in patients with obstructive hypertrophic cardiomyopathy: a word of caution.* Circ Heart Fail, 2010. **3**(3): p. 362-9.

44. Rosen KL, C.R., Bigham PJ, Neish SR., *Hypertrophic cardiomyopathy presenting with 3rd-degree atrioventricular block.* Tex Heart Inst J, 1997. **24**(4): p. 372-375.

45. Masamichi Tamura, K.H., Tadahiko Ito, Masamichi Enoki, Goro Takada, *Abrupt aggravation of atrioventricular block and syncope in hypertrophic cardiomyopathy.* Archives of Disease in Childhood 1995. **73**: p. 536-537.

46. Kaneshige T, M.N., Itoh H, Yamane Y., *The anatomical basis of complete atrioventricular block in cats with hypertrophic cardiomyopathy.* J Comp Pathol, 2006. **135**(`): p. 25-31.

47. J Kazmierczak, Z.K.-J., M Kisly, R Gil, A Wojtarowicz, *Electrocardiographic changes after alcohol septal ablation in hypertrophic obstructive cardiomyopathy.* Heart, 1998. **80**: p. 257–262.

48. Sorajja, P., et al., *Outcome of alcohol septal ablation for obstructive hypertrophic cardiomyopathy.* Circulation, 2008. **118**(2): p. 131-9.

49. Veselka, J., et al., *Outcome of patients after alcohol septal ablation with permanent pacemaker implanted for periprocedural complete heart block.* Int J Cardiol, 2014. **171**(2): p. e37-8.

50. El-Jack, S.S., et al., *Predictors of complete heart block after alcohol septal ablation for hypertrophic cardiomyopathy and the timing of pacemaker implantation.* J Interv Cardiol, 2007. **20**(1): p. 73-6.

51. Veselka, J., et al., *Long-term clinical outcome after alcohol septal ablation for obstructive hypertrophic cardiomyopathy: results from the Euro-ASA registry.* Eur Heart J, 2016. **37**(19): p. 1517-23.

52. Annabel A. Chen, M., Igor F. Palacios, MD, Theofanie Mela, MD, Danita M. Yoerger, MD, MMSc, Michael H.Picard, MD, Gus Vlahakes, MD, Patricia A. Lowry, RNCS, Michael A. Fifer, MD, *Acute Predictors of Subacute Complete Heart Block After Alcohol Septal Ablation for Obstructive Hypertrophic Cardiomyopathy.* The American Journal of Cardiology, 2006. **97**(2): p. 264-269.

53. H, S., *Current status of alcohol septal ablation for patients with hypertrophic cardiomyopathy.* Curr Cardiol Rep, 2001. **3**(2): p. 160-166.

54. Baggish, A.L., et al., *Pathological effects of alcohol septal ablation for hypertrophic obstructive cardiomyopathy.* Heart, 2006. **92**(12): p. 1773-8.

55. Foley JD 3rd, S.J., Steinhubl SR, Kolasa JR, Ebersole JL, Lin Y, Kryscio RJ, McDevitt JT, Campbell CL, Miller CS., *Salivary biomarkers associated with myocardial necrosis: results from an alcohol septal ablation model.* Oral Surg Oral Med Oral Pathol Oral Radiol, 2012. **114**(5): p. 616-623.

56. Spacek M, Z.D., Tomasov P, Veselka J, *Early opening of dormant septal collaterals during alcohol septal ablation: a possible hazard of remote necrosis.* Can J Cardiol, 2013. **29**(11): p. 1531.

57. Oto, A., et al., *Cyanoacrylate for septal ablation in hypertrophic cardiomyopathy.* Journal of interventional cardiology, 2011. **24**(1): p. 77-84.

58. Mearini, G., et al., *Repair of Mybpc3 mRNA by 5'-trans-splicing in a mouse model of hypertrophic cardiomyopathy.* Molecular Therapy-Nucleic Acids, 2013. **2**: p. e102.

59. Prondzynski, M., et al., *Evaluation of MYBPC3 trans-splicing and gene replacement as therapeutic options in human iPSC-derived cardiomyocytes.* Molecular Therapy-Nucleic Acids, 2017. **7**: p. 475-486.

60. Prondzynski, M., G. Mearini, and L. Carrier, *Gene therapy strategies in the treatment of hypertrophic cardiomyopathy.*

Pflügers Archiv-European Journal of Physiology, 2019. **471**(5): p. 807-815.

61. Behrens-Gawlik, V., et al., *MYBPC3 in hypertrophic cardiomyopathy: from mutation identification to RNA-based correction.* Pflügers Archiv-European Journal of Physiology, 2014. **466**(2): p. 215-223.
62. Ben Jehuda, R., et al., *CRISPR correction of the PRKAG2 gene mutation in the patient's iPSC-derived cardiomyocytes eliminates the electrophysiological and structural abnormalities.* Heart Rhythm, 2018. **15**(2): p. 267-276.
63. Jehuda, R.B., et al., *CRISPR correction of the PRKAG2 gene mutation in the patient's induced pluripotent stem cell-derived cardiomyocytes eliminates electrophysiological and structural abnormalities.* Heart Rhythm, 2018. **15**(2): p. 267-276.
64. Mosqueira, D., et al., *CRISPR/Cas9 editing in human pluripotent stem cell-cardiomyocytes highlights arrhythmias, hypocontractility, and energy depletion as potential therapeutic targets for hypertrophic cardiomyopathy.* European heart journal, 2018. **39**(43): p. 3879-3892.
65. Wang, L., et al., *Hypertrophic cardiomyopathy-linked mutation in troponin T causes myofibrillar disarray and pro-arrhythmic action*

potential changes in human iPSC cardiomyocytes. Journal of molecular and cellular cardiology, 2018. **114**: p. 320-327.

66. Roma-Rodrigues, C., L.R. Raposo, and A.R. Fernandes, *MicroRNAs Based Therapy of Hypertrophic Cardiomyopathy: The Road Traveled So Far.* BioMed Research International, 2015. **2015**: p. 983290.
67. Van Rooij, E. and S. Kauppinen, *Development of micro RNA therapeutics is coming of age.* EMBO molecular medicine, 2014. **6**(7): p. 851-864.
68. Thum, T., *MicroRNA therapeutics in cardiovascular medicine.* EMBO molecular medicine, 2012. **4**(1): p. 3-14.
69. Mitchell, P.S., et al., *Circulating microRNAs as stable blood-based markers for cancer detection.* Proceedings of the National Academy of Sciences, 2008. **105**(30): p. 10513-10518.
70. Care, A., et al., *MicroRNA-133 controls cardiac hypertrophy.* Nature medicine, 2007. **13**(5): p. 613-618.
71. Thum, T., et al., *MicroRNA-21 contributes to myocardial disease by stimulating MAP kinase signalling in fibroblasts.* Nature, 2008. **456**(7224): p. 980-984.

72. Ucar, A., et al., *The miRNA-212/132 family regulates both cardiac hypertrophy and cardiomyocyte autophagy.* Nature communications, 2012. **3**(1): p. 1-11.

73. Cleator, J.H., et al., *How Can we Improve Non-Surgical Septal Reduction for Hypertrophic Obstructive Cardiomyopathy?* Journal of Cardiovascular Diseases & Diagnosis, 2016.

74. Christiansen, S., et al., *Selective left ventricular adriamycin-induced cardiomyopathy in the pig.* The Journal of heart and lung transplantation, 2008. **27**(1): p. 86-92.

75. Lü, J.-M., et al., *Current advances in research and clinical applications of PLGA-based nanotechnology.* Expert review of molecular diagnostics, 2009. **9**(4): p. 325-341.

76. Katsuki, S., et al., *Anti-inflammatory nanomedicine for cardiovascular disease.* Frontiers in cardiovascular medicine, 2017. **4**: p. 87.

77. Ghitman, J., et al., *Review of hybrid PLGA nanoparticles: Future of smart drug delivery and theranostics medicine.* Materials & Design, 2020: p. 108805.

78. Matoba, T., et al., *Nanoparticle-mediated drug delivery system for atherosclerotic cardiovascular disease.* Journal of cardiology, 2017. **70**(3): p. 206-211.

79. Tsukada, Y. and H. Tsujimoto, *Development of drug-eluting stent coated with PLGA nanoparticles as drug carriers.* KONA Powder and Particle Journal, 2013. **30**: p. 2-2.

80. Chandarana, M., A. Curtis, and C. Hoskins, *The use of nanotechnology in cardiovascular disease.* Applied Nanoscience, 2018. **8**(7): p. 1607-1619.

81. Dizaj, S.M., et al., *The Application of Nanomaterials in Cardiovascular Diseases: A Review on Drugs and Devices.* Journal of Pharmacy & Pharmaceutical Sciences, 2019. **22**: p. 501-515.

82. Xi, T., et al., *In vitro and in vivo changes to PLGA/sirolimus coating on drug eluting stents.* Biomaterials, 2010. **31**(19): p. 5151-5158.

83. Indolfi, L., et al., *Microsphere-integrated drug-eluting stents: PLGA microsphere integration in hydrogel coating for local and prolonged delivery of hydrophilic antirestenosis agents.* Journal of Biomedical Materials Research Part A, 2011. **97**(2): p. 201-211.

84. Giannouli, M., et al., *Fabrication of quercetin-loaded PLGA nanoparticles via electrohydrodynamic atomization for cardiovascular disease.* Materials Today: Proceedings, 2018. **5**(8): p. 15998-16005.

85. Ohsato, K., et al., *Type IV collagen in hypertrophic cardiomyopathy.* Japanese heart journal, 1994. **35**(3): p. 311-321.

86. Kapelko, V.I., *Extracellular matrix alterations in cardiomyopathy: The possible crucial role in the dilative form.* Experimental & Clinical Cardiology, 2001. **6**(1): p. 41.

87. Maron, B.J., *Hypertrophic cardiomyopathy: a systematic review.* Jama, 2002. **287**(10): p. 1308-1320.

88. Spirito, P., et al., *The management of hypertrophic cardiomyopathy.* New England Journal of Medicine, 1997. **336**(11): p. 775-785.

89. Roberts, W.C., et al., *Severe mitral or aortic valve regurgitation, or both, requiring valve replacement for infective endocarditis complicating hypertrophic cardiomyopathy.* Journal of the American College of Cardiology, 1992. **19**(2): p. 365-371.

90. Klues, H.G., et al., *Diversity of structural mitral valve alterations in hypertrophic cardiomyopathy.* Circulation, 1992. **85**(5): p. 1651-1660.

91. Varnava, A., et al., *Hypertrophic cardiomyopathy: the interrelation of disarray, fibrosis, and small vessel disease.* Heart, 2000. **84**(5): p. 476-482.

92. Ho, C.Y., et al., *Myocardial fibrosis as an early manifestation of hypertrophic cardiomyopathy.* New England Journal of Medicine, 2010. **363**(6): p. 552-563.

93. Urbano-Moral, J.A., et al., *Investigation of global and regional myocardial mechanics with 3-dimensional speckle tracking echocardiography and relations to hypertrophy and fibrosis in hypertrophic cardiomyopathy.* Circulation: Cardiovascular Imaging, 2014. **7**(1): p. 11-19.

94. Hinojar, R., et al., *Prognostic implications of global myocardial mechanics in hypertrophic cardiomyopathy by cardiovascular magnetic resonance feature tracking. Relations to left ventricular hypertrophy and fibrosis.* International journal of cardiology, 2017. **249**: p. 467-472.

95. Rezakhaniha, R., et al., *Experimental investigation of collagen waviness and orientation in the arterial adventitia using confocal laser scanning microscopy.* Biomechanics and modeling in mechanobiology, 2012. **11**(3-4): p. 461-473.

96. Fujiwara, H., et al., *Number and size of myocytes and amount of interstitial space in the ventricular septum and in the left ventricular free wall in hypertrophic cardiomyopathy.* The American journal of cardiology, 1983. **52**(7): p. 818-823.

97. Unverferth, D.V., et al., *Regional myocyte hypertrophy and increased interstitial myocardial fibrosis in hypertrophic*

cardiomyopathy. The American journal of cardiology, 1987. **59**(9): p. 932-936.

98. Abdallah, M.-N., et al., *Biomaterials used in orthodontics: brackets, archwires, and clear aligners*, in *Advanced Dental Biomaterials*. 2019, Elsevier. p. 541-579.

99. Szczesny, S.E. and D.M. Elliott, *Interfibrillar shear stress is the loading mechanism of collagen fibrils in tendon.* Acta biomaterialia, 2014. **10**(6): p. 2582-2590.

100. Coffin, D. and C. Fellers, *Paper: Creep.* Encyclopedia of Materials: Science and Technology. Elsevier Science Ltd, 2001: p. 6656-6659.

101. Ahmad, F., et al., *Biomechanical properties and microstructure of neonatal porcine ventricles.* Journal of the mechanical behavior of biomedical materials, 2018. **88**: p. 18-28.

102. Holzapfel, G.A., G. Sommer, and P. Regitnig, *Anisotropic mechanical properties of tissue components in human atherosclerotic plaques.* J. Biomech. Eng., 2004. **126**(5): p. 657-665.

103. Humphrey, J., R. Strumpf, and F. Yin, *Determination of a constitutive relation for passive myocardium: I. A new functional form.* 1990.

104. Novak, V.P., F. Yin, and J. Humphrey, *Regional mechanical properties of passive myocardium.* Journal of biomechanics, 1994. **27**(4): p. 403-412.

105. Humphrey, J. and F. Yin, *On constitutive relations and finite deformations of passive cardiac tissue: I. A pseudostrain-energy function.* 1987.

106. Valdez-Jasso, D., et al., *A murine experimental model for the mechanical behaviour of viable right-ventricular myocardium.* The Journal of physiology, 2012. **590**(18): p. 4571-4584.

107. Purslow, P.P., T.J. Wess, and D. Hukins, *Collagen orientation and molecular spacing during creep and stress-relaxation in soft connective tissues.* Journal of Experimental Biology, 1998. **201**(1): p. 135-142.

108. Akinori Kimura, H.H., Jeong-Euy Park, Hirofumi Nishi, Manatsu Satoh,, et al., *Mutations in the cardiac troponin I gene associated with hypertrophic cardiomyopathy* Nat Genet., 1997. **16**(4): p. 379-382.

109. Maron, B.J., M.S. Maron, and C. Semsarian, *Genetics of hypertrophic cardiomyopathy after 20 years: clinical perspectives.* J Am Coll Cardiol, 2012. **60**(8): p. 705-15.

110. Kraft, T., et al., *Familial hypertrophic cardiomyopathy: functional effects of myosin mutation R723G in cardiomyocytes.* J Mol Cell Cardiol, 2013. **57**: p. 13-22.

111. Helling, A., et al., *In vitro enzymatic degradation of tissue grafts and collagen biomaterials by matrix metalloproteinases: improving the collagenase assay.* ACS Biomaterials Science & Engineering, 2017. **3**(9): p. 1922-1932.

112. Zinger, A., et al., *Collagenase nanoparticles enhance the penetration of drugs into pancreatic tumors.* ACS nano, 2019. **13**(10): p. 11008-11021.

113. Murty, S., et al., *Nanoparticles functionalized with collagenase exhibit improved tumor accumulation in a murine xenograft model.* Particle & Particle Systems Characterization, 2014. **31**(12): p. 1307-1312.

114. Villegas, M.R., A. Baeza, and M. Vallet-Regí, *Hybrid collagenase nanocapsules for enhanced nanocarrier penetration in tumoral tissues.* ACS applied materials & interfaces, 2015. **7**(43): p. 24075-24081.

115. Goncalves, G.K., T.H.C. de Oliveira, and N. de Oliveira Belo, *Cardiac hypertrophy and brain natriuretic peptide levels in an*

ovariectomized rat model fed a high-fat diet. Medical science monitor basic research, 2017. **23**: p. 380.

116. Mukhopadhyay, P., et al., *Role of superoxide, nitric oxide, and peroxynitrite in doxorubicin-induced cell death in vivo and in vitro.* American Journal of Physiology-Heart and Circulatory Physiology, 2009. **296**(5): p. H1466-H1483.

117. Barenholz, Y.C., *Doxil®—the first FDA-approved nano-drug: lessons learned.* Journal of controlled release, 2012. **160**(2): p. 117-134.

118. Bagnall, R.D., et al., *Whole genome sequencing improves outcomes of genetic testing in patients with hypertrophic cardiomyopathy.* Journal of the American College of Cardiology, 2018. **72**(4): p. 419-429.

119. Marian, A. and R. Roberts, *The molecular genetic basis for hypertrophic cardiomyopathy.* Journal of molecular and cellular cardiology, 2001. **33**(4): p. 655-670.

120. Maron, B.J., E.J. Rowin, and M.S. Maron, *Global burden of hypertrophic cardiomyopathy.* JACC: Heart Failure, 2018. **6**(5): p. 376-378.

121. O'Mahony, C., et al., *A novel clinical risk prediction model for sudden cardiac death in hypertrophic cardiomyopathy (HCM risk-SCD).* European heart journal, 2014. **35**(30): p. 2010-2020.

122. ALAM, M., H. DOKAINISH, and N. LAKKIS, *Alcohol septal ablation for hypertrophic obstructive cardiomyopathy: a systematic review of published studies.* Journal of interventional cardiology, 2006. **19**(4): p. 319-327.

123. Baggish, A.L., et al., *Pathological effects of alcohol septal ablation for hypertrophic obstructive cardiomyopathy.* Heart, 2006. **92**(12): p. 1773-1778.

124. Firoozi, S., et al., *Septal myotomy–myectomy and transcoronary septal alcohol ablation in hypertrophic obstructive cardiomyopathy. A comparison of clinical, haemodynamic and exercise outcomes.* European Heart Journal, 2002. **23**(20): p. 1617-1624.

125. Zhao, W., et al., *A murine hypertrophic cardiomyopathy model: the DBA/2J strain.* PloS one, 2015. **10**(8).

BIOGRAPHICAL INFORMATION

Katherine McGrath Copeland was born October 22, 1992 in Jackson, MS. She attended Mississippi State University and graduated with a bachelor's degree in Microbiology in 2015. After graduation, Katherine joined Dr. Jun Liao's lab group in the Tissue Biomechanics and Bioengineering Laboratory at Mississippi State University. In 2017, Katherine moved to Arlington, TX with her husband and two children to finish her Ph.D. studies under Dr. Liao at the University of Texas at Arlington. Katherine was selected as an NIH T32 fellow in the fall of 2017 under the advisement of Dr. Kytai Nguyen. Katherine successfully defended her dissertation on August 21, 2020.